CENTRO DE INVESTIGACIONES EN ÓPTICA, A.C.

ENGINEERING OF FOCAL FIELDS USING VECTORIAL OPTICAL FIELDS

(Final version, changes suggested by advisors are included)

MAESTRÍA EN CIENCIAS (ÓPTICA)

Advisor: Dr. Rafael Espinosa Luna ***Co-advisor: Dr. Qiwen Zhan***

Student: Ing. Jason Eduardo Gómez Jamaica

January 2017
León, Guanajuato, México

Dedicatory

Este trabajo es dedicado a mi querida familia, es decir, mi padre quien siempre ha estado cuando lo necesito y que sin importar las circunstancias me da ánimos para seguir adelante, mi madre quien siempre ha hecho y dado todo para que yo esté bien y mis hermanos Jonathan, Jeremy y Jacob quienes son lo más querido y para quienes siempre estaré.

Acknowledgments

Firstly, I would like to thank to the Consejo Nacional de Ciencia y Tecnología, CONACyT, for scholarship (339087) that made possible my Master's degree. On the other hand, I also render thanks to the Centro de Investigaciones en Óptica, A.C., for the academic preparation that I obtained and I want to thank specially to my advisor Dr. Rafael Espinosa Luna, my co-advisor Dr. Qiwen Zhan, my thesis reviewers Dr. Francisco Villa Villa and Dr. Moisés Cywiak Garbarcewicz, my professor Dr. Alejandro Téllez Quiñones, my classmates Oscar Naranjo, Etna Yáñez , Alan Bernal, Guadalupe López, Izcoatl Saucedo, Alan López, Eduardo Rocko, Carlos Zamarripa, my friends Victor, Eusebio, Francisco, Wilson, Diana and Felipe, and the admirable Dr. Efrain Mejia Beltran, which were a great support for me.

Abstract

In this work is presented a revision of the main four theoretical methods employed for the generation of longitudinally polarized beams of light. Results obtained by numerical simulations using the method we consider the closest to our experimental capabilities are presented. The source employed has associated an unconventional polarization distribution corresponding to a radial polarization mode and although one can generate longitudinally polarized beams by focusing a radially polarized light source with an aplanatic lens of high numerical aperture, the strength of the longitudinal field component of these beams decreases rapidly outside their waist. Therefore, we also present by numerical simulations techniques to enhance the longitudinal field component of these beams, where different radially polarized light sources were impinged on an annular diffractive optical element of binary phase and then focused in a set-up of aplanatic high numerical aperture lenses, and depending on the characteristics of the light source, the geometry of the diffractive optical element, and the numerical aperture of the lenses, will be the beam dimensions and its intensity profile. Thus, we achieved to obtain a non-diffracting longitudinally polarized beam with FWHM=3.1λ, constant waist (0.88 λ) and a flat profile over most the covered intensity area. Additionally, we have proposed an experimental method to verify the existence of numerically simulated longitudinally polarized beams.

Table of contents

Symbols

Symbol	Description	Value and/or units
$\lvert\vec{\mathrm{E}}\rvert$	Electric field	$\mathrm{V/m}$
$\lvert\vec{\mathrm{D}}\rvert$	Electric displacement field	$\mathrm{C/m^2}$
$\lvert\vec{\mathrm{H}}\rvert$	Intensity of magnetic field	$\mathrm{A/m}$
$\lvert\vec{\mathrm{B}}\rvert$	Induction of magnetic field	T
$\lvert\vec{\mathrm{J}}\rvert$	Electric current density	$\mathrm{A/m^2}$
$\lvert\vec{S}\rvert$	Poynting vector	$\mathrm{W/m^2}$
$\lvert\vec{F}\rvert$	Force	N
$\lvert\vec{v}\rvert$	instantaneous velocity of an electric charge	$\mathrm{m/s}$
v	Speed of a wave through a medium	$\mathrm{m/s}$
c	Speed of light in the vacuum	$3\mathrm{x}10^8\ \mathrm{m/s}$
λ	Wavelength	m
σ	Electric conductivity	$\mathrm{S/m}$
μ	Magnetic permeability	$\mathrm{H/m}$
ε	Electrical permittivity	$\mathrm{F/m}$
ρ_q	Electric charge density	$\mathrm{C/m^3}$
t	Time	s
q	Electric charge	C
ρ_ξ	Energy density	$\mathrm{J/\ m^3}$
I_{pp}	Intensity of the partially polarized light	W
I_{cp}	Intensity of the completely polarized light	W

Abbreviations

CV	Cylindrical Vector
DOF	Depth of Focus
BG	Bessel-Gaussian
NA	Numerical Aperture
DOE	Diffractive Optical Element
FWHM	Full Width at Half Maximum
3D	Three-Dimensional
PP	Polarization Plane
FF	Focal Field
ULS	Uniform Line Source
XZP	xz-plane
MO	Microscopy Objective
S-WP	S-Waveplate

Chapter 1

Introduction.

---

1. Introduction.

The polarization properties of light have been used as tools for different purposes, ranging from basic research to application areas. Similarly, since the polarization can be roughly divided in two types, conventional and unconventional polarization, the applications areas are also divided. Therefore, one of the polarization modes in the unconventional polarization is the mode with radial polarization. Where these beams are currently used in three-dimensional focus engineering and due to its unusual properties, these beams have been highly applied in research areas as optical trapping and manipulation, particles acceleration, confocal microscopy, fluorescent imaging, second-harmonic generation, Raman spectroscopy and high-density optical data storage. Thus, the generation of specific focal fields has been reported theoretically by employing four different methods, which use very sophisticated techniques.

The first method consists of the incidence of a radially polarized Bessel-Gaussian beam on a diffractive optical element to then be focused with a high numerical aperture aplanatic-lens, and so it is generated, in the depth of focus region, a longitudinally polarized optical needle with constant waist and length of 0.43λ and 4λ, respectively, which are dependent both of the numerical aperture and diffractive optical element geometry [1, 2]. The second method consists of a focusing system, where radially polarized beams are focused to create a spherical focal spot in the focal region of the focusing system, in which different optical elements are analyzed in order to generate focal spots with different profile shape [3, 4]. The third method consist of the generation of a longitudinally polarized beam with super-Gaussian profile and constant waist of 0.36λ, where these beams are generated by an incident radially polarized beam in the optical arrangement with an annular paraboloid mirror and a special filter, where it can be modulated its structural parameters in order to generate a light needle (flat-top beam) length until 10λ [3, 4]. The last method consists in obtaining a light needle with waist and length up to 0.36λ and 9.24λ, respectively, where the light needle is generated by reversing the electric field pattern radiated from a different antennas in a 4Pi focusing system, and depending on the numerical aperture of the aplanatic lenses of the 4Pi focusing system and the

type and characteristics of the antenna, will be the dimensions of the generated light needle [2].

Therefore, in order to propose an attainable and experimental method for generating specific focal fields and at the same time verify the generated focal field by numerical simulations, we studied in this thesis the four theoretical methods for generating these fields, therefore we proposed a new and different method, which consists of an incoming beam in a polarization converter and so this has a radial polarization; when the beam is radially polarized, this passes through two optical elements, a concentric two-belts diffractive optical element and a microscope objective with numerical aperture of 0.90, and then is generated a longitudinally polarized beam with flat intensity profile over most of the covered area, in other words, a light needle is generated, which is located along the depth of field region (DOF). Thus, if the light is generated in the depth of focus of the microscopy objective, we could verify the existence of the light needle by using a vision system, consisting on a CMOS camera and an image forming lens, where this system can be displaced along the optical axis in order to verify the focal field formed in the DOF, so this field could be scanned registering the images of the object at different positions.

Chapter 2
Introduction to the polarization of light.

---

2. Introduction to the polarization of the light.

One of the keywords in this work is "polarization of light", therefore, before its definition, a short description of its origin will be provided.

Physics is the science focused to the study of the behavior and properties of matter and energy, and interaction between them. Physical studies are divided in branches that are, mechanics, thermodynamics, acoustics, electromagnetism, optics, and modern physics. Optics studies the light and its interaction with matter. Depending on the conditions of the generation and propagation of light and its interaction with matter, it is divided in three big branches, which are, geometric optics, physics optics, and optoelectronics. Each branch analyzes the beam differently, namely, like a propagating ray in the case of the geometric optics, like a particle (photon) in the case of the optoelectronics and finally, like a wave in the case of the optical physics approximation.

In this thesis, the polarization of light will be described using the physical optics approximation, where the light is considered as a monochromatic plane traveling wave and whose interactions with matter involve only linear optical responses.

For the study of the physical optics approximation, the beam is studied more specifically like an electromagnetic wave. This electromagnetic wave can be represented as the combination of two vectorial fields. The electric "E" and magnetic "H" fields. These fields are mutually perpendicular and orthogonal to the propagation vector "S" of the wave Fig. (1), and it is supposed that the electromagnetic waves are propagated in the vacuum, or another dielectric media.

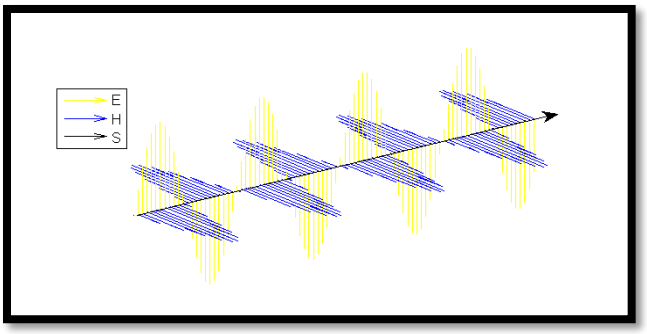

Figure 1. Representation of the orthogonal vector field components, $\vec{\mathrm{E}}$ and $\vec{\mathrm{H}}$, in an electromagnetic wave propagating along the $\vec{S}$ direction.

The propagation vector is well-known as Poynting vector $\vec{S}$ and whose modulus $|\vec{S}|$ represents the instantaneous intensity of the electromagnetic energy that flows through a surface perpendicular to the propagation direction of the wave:

$$\vec{S} = \vec{E} \times \vec{H} \,. \tag{2.1}$$

The electromagnetic waves can have a property that will be named "Polarization", that takes account of the orientation of the electric and magnetic field as the wave propagates in the space.

Although the magnetic field could be used to represent the polarization of light, the main reason to using only the electric field is that the strength of electric field is "c" times the field strength of magnetic intensity field. Namely, the interaction of the magnetic field at optical frequencies is rather weak so, the value of the energy density and the force (Lorentz force) exerted by electromagnetic fields, ρ_ξ and $\vec{F}$ respectively, have much greater contribution due to the electric field:

$$\rho_\xi = \frac{1}{2}\left(\vec{E} \cdot \vec{D} + \vec{B} \cdot \vec{H}\right). \tag{2.2}$$

$$\vec{F} = q\left(\vec{E} + \vec{v} \times \vec{B}\right). \tag{2.3}$$

Where $\vec{D}$ and $\vec{B}$ represent the displacement vector and the magnetic induction, q is the electric charge, and $\vec{v}$ is the instantaneous velocity vector of the electric charge.

2.1. Spatially uniform polarization states (conventional polarization)

Since the light is an electromagnetic wave that has a dependence in space and time, is possible describe it in terms of the electric field $\vec{E}$. Thus, the electric field can be taken as the superposition of the two mutually orthogonal fields, $\overrightarrow{E_x}$ and $\overrightarrow{E_y}$, that travel on the same direction and whose phase difference, $\delta_x - \delta_y$, determines the polarization state.

$$\vec{E} = \overrightarrow{E_x} + \overrightarrow{E_y}\,. \tag{2.1.1}$$

The $\overrightarrow{E_x}$ and $\overrightarrow{E_y}$ vectors oscillate on the xz and yz planes, respectively.

$$\overrightarrow{E_x} = E_{0x}\, e^{i(\omega t - kz + \delta_x)}\, \widehat{e_x}\,. \tag{2.1.2}$$

$$\overrightarrow{E_y} = E_{0y}\, e^{i(\omega t - kz + \delta_y)}\, \widehat{e_y}\,. \tag{2.1.3}$$

Thus, the electric field $\vec{E}$ has associated an angular frequency ω and a wavenumber k. On the other hand, $\vec{E}$ also has temporal t and spatial z dependence, so $\vec{E}$=$\vec{E}(t,z)$, and E_{0x}, δ_x, $\widehat{e_x}$ and E_{0y}, δ_y, $\widehat{e_y}$ are the amplitudes, phases and unit vectors of the $\overrightarrow{E_x}$ and $\overrightarrow{E_x}$ fields, respectively.

The trajectory described by the end of the electric field in the space can be described alternatively at a fixed point as a function of time, or it can be described at a fixed time as a function of the spatial coordinates. The polarization of the light can be classified into five categories, which are known as “polarization states” with spatially uniform distributions of the amplitude and phase.

Linear polarization (first category).

The linearly polarized state can be described as the superposition of two orthogonal electric fields, $\overrightarrow{E_x}$ and $\overrightarrow{E_x}$, traveling along the same direction S (propagation vector) and having a phase difference δ of 0 degrees, that is, $\delta_y - \delta_x = 0$. On the other hand, the electric field $\vec{E}$ oscillates along a same plane, which will be named PP (polarization plane) and the value of the amplitudes of the $\overrightarrow{E_x}$ and $\overrightarrow{E_x}$ fields will depend on the orientation of the polarization plane around the optical axis z, where all the electric field vectors oscillate on the polarization plane, which is fixed to an angle θ with respect to the XZP (xz-plane), described within a Cartesian coordinate system (x, y, z). This description is reported observing to the source.

For simplicity, the direction of the S vector has been chosen to be parallel to the z axis Fig. (2).

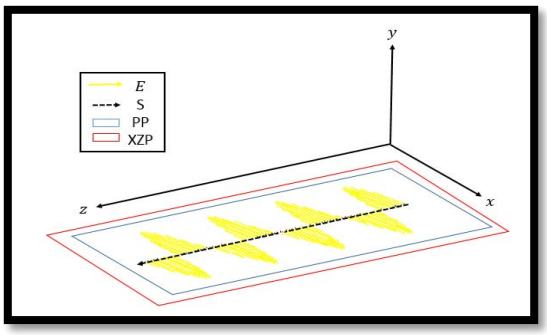

a) Linear (p)-polarization state

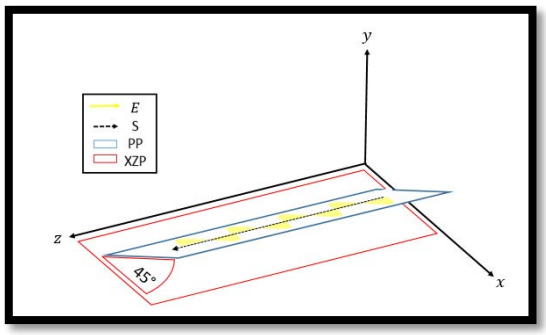

b) Linear (+45 degrees)-polarization state

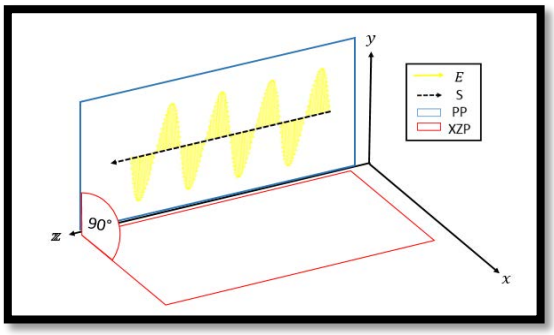

c) Linear (s)-polarization state

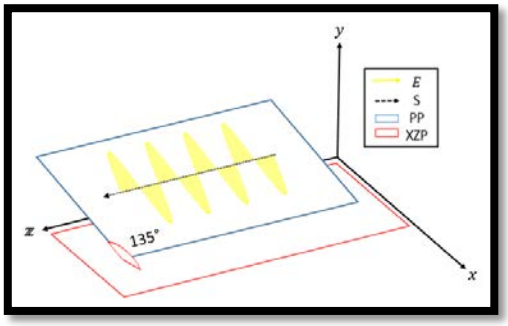

d) Linear (-45 degrees)-polarization state

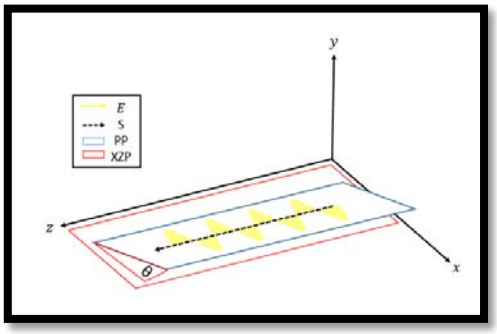

e) Linear (θ)-polarization state

Figure 2. Linearly polarized states under different tilt angles of the polarization plane (considering the tilt angles of the polarization plane with respect to the XZP). a) PP to 0 degrees, where this polarization state is well-known as (p)-polarization and (p) means *paralelle*, which comes from the German language. b) PP to 45 degrees, where this polarization state is known as (+45 degrees)-polarization and (+45 degrees) stands for the tilt angle of the PP to 45 degrees. c) PP to 90 degrees, where this polarization state is well-known as (s)-polarization and (s) means *senkrecht*, which comes from the German language. d) PP to -45 degrees, where this polarization state is known as (-45 degrees)-polarization and (-) stands for the tilt of the PP to 45 degrees. e) PP to a θ (any angle), where this polarization state is known as (θ)-polarization and θ stands for the tilt of the PP to a θ.

Circular polarization (Second category).

The circularly polarized state can be described as the superposition of the two orthogonal electric fields, $\overrightarrow{E_x}$ and $\overrightarrow{E_y}$, with equal amplitudes $(E_x = E_y)$, traveling along the same direction, and whose phase difference δ between the orthogonal electric components is of $\pm$90 degrees. If the value of δ is +90 degrees, $\overrightarrow{E_x}$ and $\overrightarrow{E_y}$ rotates at clockwise, and the resultant electric field $\vec{E}$ describes a complete circle after a period of a wavelength; this state is named "circular right-hand polarization". Otherwise, If the δ is -90 degrees, $\overrightarrow{E_x}$ and $\overrightarrow{E_y}$ rotate at counter-clockwise, and the resultant electric field describes a complete circle after a period of a wavelength; this state is named "circular left-hand polarization". On the other hand, the electric field $\vec{E}$ oscillates along a different plane, which will be named PP (polarization plane) and depending of the value of the amplitudes of the $\overrightarrow{E_x}$ and $\overrightarrow{E_x}$ fields, will be the orientation of the polarization plane around the optical axis z. Therefore, for each electric field vectors $\vec{E}$, there is a single polarization plane, that is, a E vector set, where each one of them will be located on a polarization plane to an angle θ with respect to the XZP (xz-plane), described within a Cartesian coordinate system (x, y, z). This description is reported observing to the source.

The aforementioned E vector set is generated by the angular motion of a single vector E that traveling along the z optical axis. This motion can be modeled completely as a cylindrical helix with constant radius, that is, a helical motion.

Note that the direction of the S vector is along the z axis Fig (3).

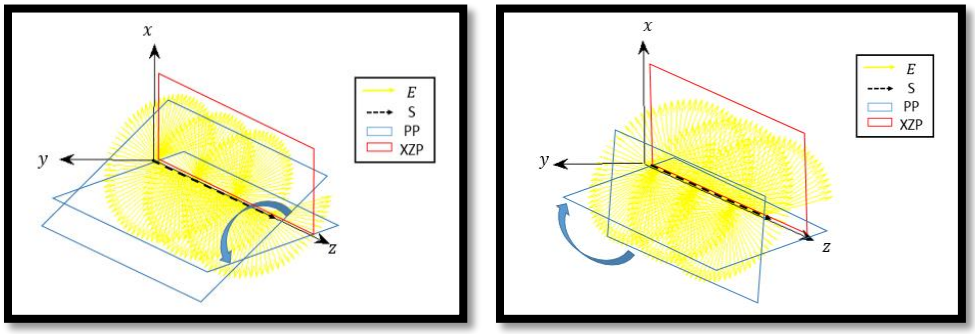

a) Circular (L)-polarization state b) Circular (R)-polarization state

Figure 3. Circularly polarized states with both rotations. a) Circular polarization state at counter-clockwise with respect to the S direction, where this polarization state is well-known as (L)-polarization and "L" stands for "Left hand", which means that the E vector rotates at counter-clockwise. b) Circular polarization state at clockwise with respect to the S direction, where this polarization state is well-known as (R)-polarization and "R" stands for "Right hand", which means that the E vector rotates clockwise.

Elliptical polarization (third category).

The elliptically polarized state can be described as the superposition of the two orthogonal electric fields, $\overrightarrow{E_x}$ and $\overrightarrow{E_y}$, with different amplitudes $(E_x \neq E_y)$, traveling along the same direction, and whose phase difference δ between the orthogonal electric components, can take any value, except 0 and ∓ 90 degrees. If the value of δ is positive, $\overrightarrow{E_x}$ and $\overrightarrow{E_y}$ rotates clockwise, and the resultant electric field $\vec{E}$ describes a complete circle after a period of a wavelength; this state is named "elliptical right-hand polarization". Otherwise, If the δ is negative, $\overrightarrow{E_x}$ and $\overrightarrow{E_y}$ rotate counter-clockwise, and the resultant electric field describes a complete ellipse after a period of a wavelength; this state is named "elliptical left-hand polarization". The electric field $\vec{E}$ oscillates in a plane called the PP. Therefore, for each electric field vector $\vec{E}$, there will be a single PP, that is, a E vector set where each one of them will be located on a PP to different slope with respect to the XZP (xz-plane), described within a Cartesian coordinate system (x, y, z). This description is reported observing to the source.

The aforementioned E vector set is generated by the angular motion of a single vector E traveling along the z optical axis. This motion can be modeled completely as a cylindrical helix with variable radius, that is, a helical motion.

Note that the direction of the S vector is along the z axis Fig. (4).

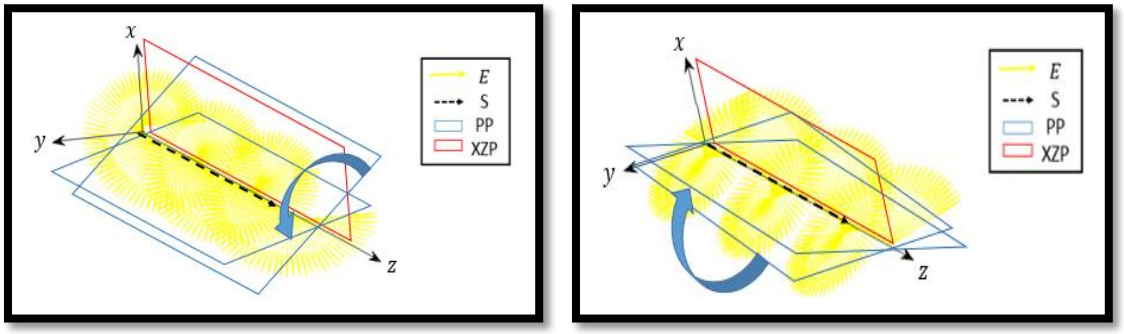

a) Elliptical left-hand polarization state b) Elliptical right-hand polarization state

Figure 4. Elliptically polarized states with both rotations with respect to the S vector direction. a) Elliptically polarized state at counter-clockwise sense, where this polarization state is well-known as "left hand elliptical polarization state", which means that the E vector rotate at counter-clockwise sense. b) Elliptical polarization state at clockwise sense, where this polarization state is well-known as "Right hand elliptical polarization state", which means that the E vector rotate at clockwise sense.

Partially polarized state (fourth category).

According to the last statement, although the polarized light can be classified by its polarization states, this is not always completely polarized, which means that the path traced by a part of the electric field is not completely defined. This restriction implies that only a portion of the light is completely polarized, in other words, the light is partially

polarized or is not completely polarized. Therefore, the combination between a completely polarized state and an unpolarized state, results a partially polarized state, which has associated a DoP (degree of polarization) and can be represented by:

$$S = \begin{pmatrix} S_0 \\ S_1 \\ S_2 \\ S_3 \end{pmatrix} = (1 - DoP) \begin{pmatrix} S_0 \\ 0 \\ 0 \\ 0 \end{pmatrix} + DoP \begin{pmatrix} S_0 \\ S_1 \\ S_2 \\ S_3 \end{pmatrix}. \quad (2.1.4)$$

Where S_0, S_1, S_2 and S_3 are elements of the Stokes vector, in which the S_1, S_2 and S_3 parameters represent a specific polarization state with total intensity indicated by the S_0 parameter. On the other hand, the DoP for completely polarized light is one (DoP=1), for unpolarized light the DoP is zero (DoP=0), and as mentioned above, for partially polarized light the DoP varies between zero and one (0 < DoP < 1). Thus, the DoP can be represented mathematically as:

$$DoP = \frac{I_{cp}}{I_{pp}} = \frac{\sqrt{{S_1}^2 + {S_2}^2 + {S_3}^2}}{S_0}. \quad (2.1.5)$$

Where I_{pp} and I_{cp} are the intensities of the partially and completely polarized light, respectively. Therefore, if the light is completely or partially polarized, the Stokes vector parameters meet certain relationships between them:

Completely polarized light $\quad {S_0}^2 = {S_1}^2 + {S_2}^2 + {S_3}^2$. $\quad (2.1.6)$

Partially polarized light $\quad {S_0}^2 > {S_1}^2 + {S_2}^2 + {S_3}^2$. $\quad (2.1.7)$

Non-polarized state (last category).

Thus, the behavior and the description of the electric field of light by the end is known as “polarization of the light” and is represented by the path traced the electric field vector. However, when the path traced by the electric field describes a random orientation, it is said that light is not polarized, which means that amplitude and phase vary randomly in space and time.

2.2. The Poincarè sphere

As previously stated above, the polarization states can be represented by the Stokes vector, which can be written as:

$$S = \begin{pmatrix} S_0 \\ S_1 \\ S_2 \\ S_3 \end{pmatrix}. \quad (2.2.1)$$

Whose parameters can be represented like a point that is located in a sphere, which is named “Poincarè sphere”, Fig. (5).

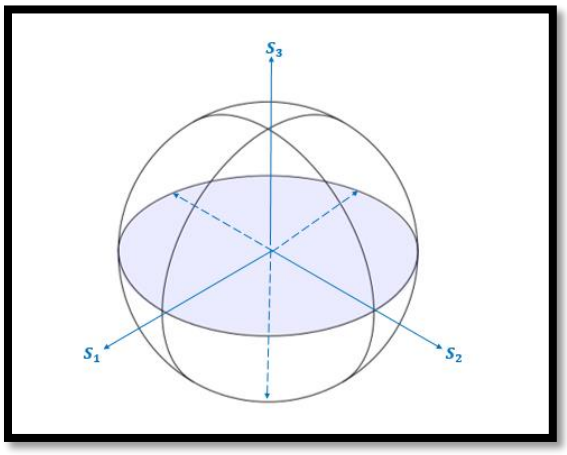

Figure 5. Representation of the Poincarè sphere

Where S_1, S_2 and S_3 are parameters that indicate the values of the axes in a sphere, with an unity radius.

Then, for a totally polarized state, the point (s_1,s_2,s_3) is on the surface of the sphere and for a partially polarized state, the point (s_1,s_2,s_3) is inside it. Another way to represent a polarization state in the Poincarè sphere, is by means of the orientation and ellipticity angles, ψ and χ, respectively, which can be represented in the sphere as shown in the following figure.

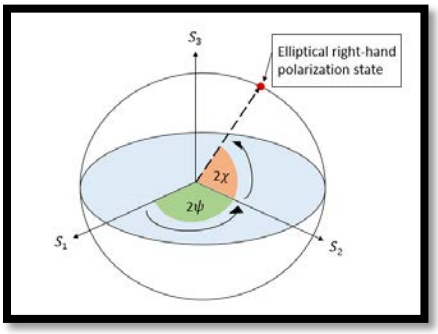

Figure 6. Representation of the ψ and χ angles in the Poincarè sphere.

Where ψ and χ are angles that depend also of the amplitudes and phases of the orthogonal components of the electric field, and they can be represented mathematically as:

$$\tan(2\psi) = 2\frac{E_{0x}E_{0y}}{{E_{0x}}^2 - {E_{0y}}^2}\cos(\delta)\ . \qquad (2.2.2)$$

With $(0 \leq \psi \leq \pi)$.

$$\sin(2\chi) = 2\frac{E_{0x}E_{0y}}{{E_{0x}}^2 + {E_{0y}}^2}\sin(\delta)\ . \qquad (2.2.3)$$

With χ between - $\pi/4$ and $\pi/4$, that is, $\left(-\frac{\pi}{4} \leq \chi \leq \frac{\pi}{4}\right)$.

2.3. Spatially non-uniform polarization modes (unconventional polarization).

In optics, when one analyzes a polarization state of light, it also is usually assumed that the cross section of the light beam has spatially homogeneous polarization, that is, the polarization is studied conventionally. However, there are beams whose polarization is not spatially homogeneous and this property of light gave rise to new phenomena and applications, in what is called unconventional polarization.

As it was previously mentioned, the path traced by the end of the electric field can be represented by polarization states, where the spatial distribution of the electric field is uniform, that is, all electric field vectors associated with each point on a lighting region (light spot), have equal direction and sense Fig. (1). Thus, when the inner product between an arbitrary vector and all $\vec{E}$ is equal to the product of the modules of said vectors, the polarization is known as conventional, that is, “Conventional polarization”.

Assuming that the degree of polarization is unity (DoP=1).

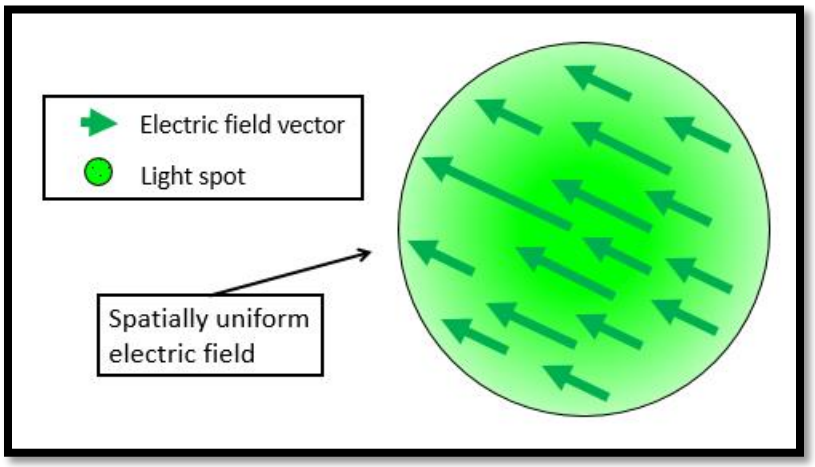

Figure 1. Conventional polarization

However, the spatial distribution of the electric field, it is not always uniform, entailing to the existence of a new type of polarization, which is known as “Non-conventional polarization” Fig. (2), where not all vectors of the field $\vec{E}$ have equal direction and sense, implying that the inner product between an arbitrary vector and any other element of the vectorial field $\vec{E}$ is different to the product of the modules of said vectors.

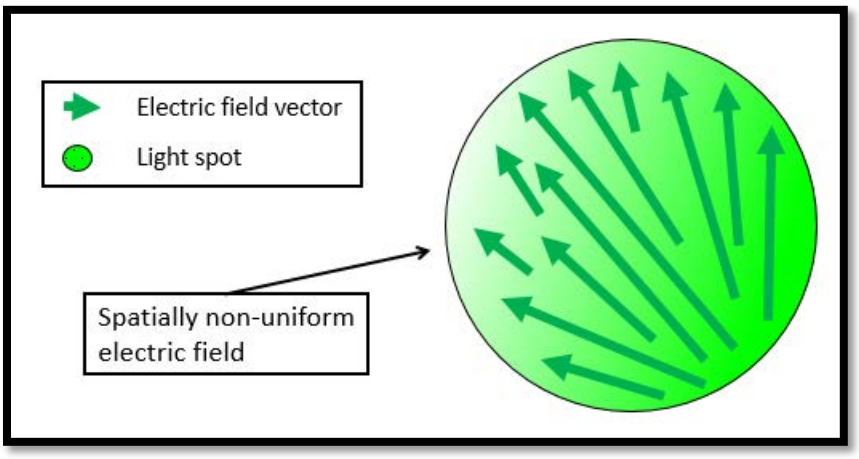

Figure 2. Unconventional polarization

Thus, the linear superposition of light with unconventional polarization generates unconventional polarization states, which are known as polarization modes and are spatially non-uniform. An elementary Gaussian beam with linear polarization has oriented its electric field components along a unique direction and sense, see Fig. 3(a). In contrast to the best known spatial distributions, which are the Hermite-Gauss (HG) and the Laguerre-Gauss (LG) modes with linear polarization, with their electric field vectors oscillating in same direction but in different sense, Figs. 3(b)-3(f). Of particular importance to us, are the unconventional distributions with electric field vectors directed around the radial and the azimuthal direction, which are named modes with radial and azimuthal polarization, respectively, and are represented in Figs. 3(g) and 3(h); when these two modes are superimposed linearly, they give rise to the mode with spiral polarization, which is found in the Fig. 3(i) and represented the unconventional state of a generalized cylindrical vector-beam [19].

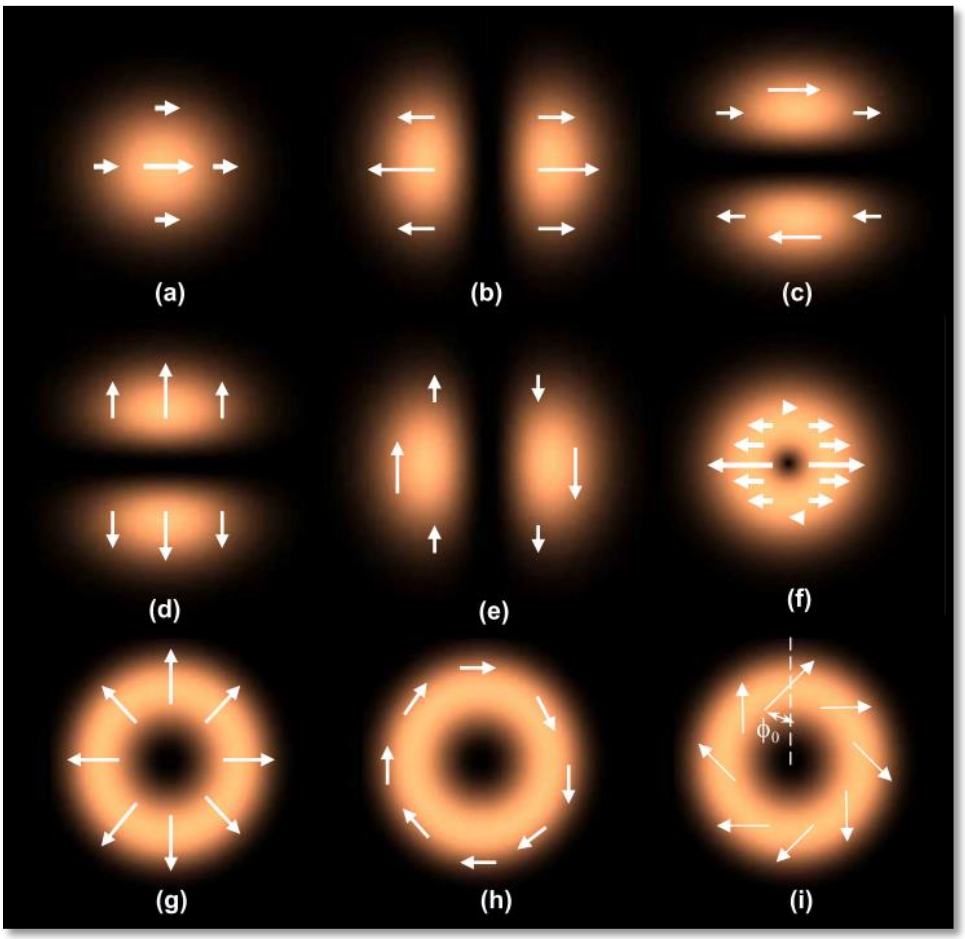

Figure 3. Best known spatially non-uniform polarization modes compared with the polarization state of an elementary Gaussian beam: (a) x-polarized elementary Gaussian beam, (b) x-polarized HG_{10} mode, (c) x-polarized HG_{01} mode, (d) y-polarized HG_{01} mode, (e) y-polarized HG_{10} mode, (f) x-polarized LG_0 mode, (g) mode with radial polarization, (h) mode with azimuthal polarization, (i) mode with spiral polarization. Figure taken from [19].

The subscripts of the HG modes indicate the degree of the probabilistic Hermite polynomials both x and y; in the same way, the subscript of the LG mode indicates the degree of the generalized Laguerre polynomials $L^1(\cdots)$.

Similarly, the radially and azimuthally polarized modes are represented as the linear superposition of a x-polarized HG_{10} mode with a y-polarized HG_{01} mode and a x-polarized HG_{01} mode and a y-polarized HG_{10} mode, respectively, which shown in Fig. (4) and can be represented mathematically as [19]:

$$\vec{E}_r = HG_{10}\,\vec{e}_x + HG_{01}\,\vec{e}_y\,. \tag{2.3.1}$$

$$\vec{E}_\phi = HG_{01}\,\vec{e}_x + HG_{10}\,\vec{e}_y\,. \tag{2.3.2}$$

Where $\vec{E}_r$ and $\vec{E}_\phi$ are electric fields with radial and azimuthal polarization, respectively.

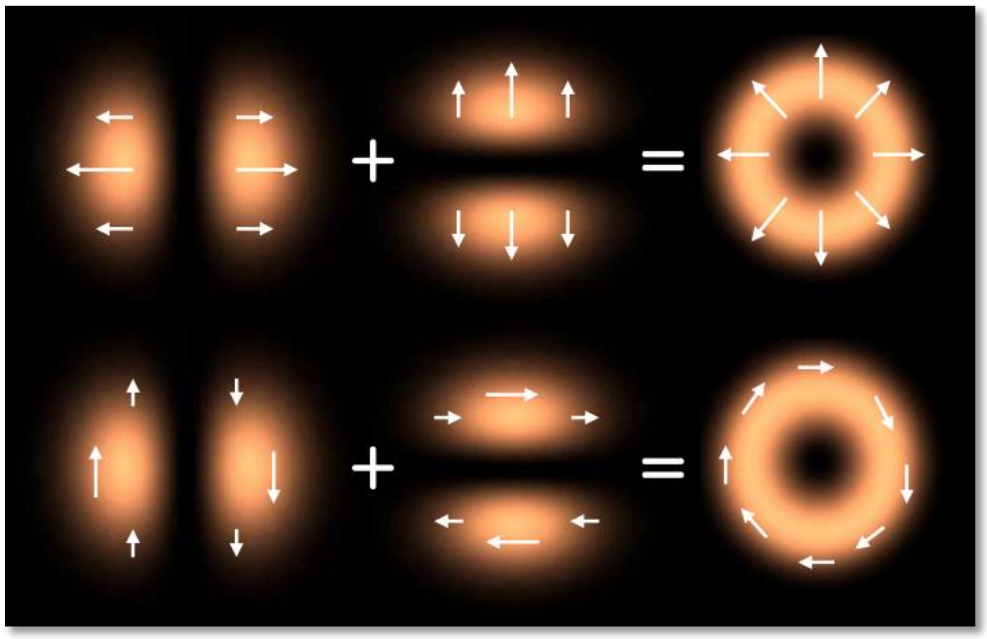

Figure 4. Radially and azimuthally polarized modes by the linear superposition of the different HG modes. Figure taken from [19].

2.4. Jones and Stokes matricial formalisms.

The light (electromagnetic waves) can be classified in terms of its polarization state, and it is possible to represent the light mathematically by two different formalisms known as Jones and Stokes matricial formalisms.

Jones matrix formalisms (first formalism).

In this formalism the polarization states of the totally polarized light are represented as a column vectors of dimensions 2×1, which can be represented by the orthogonal components, $\overrightarrow{E_x}$ and $\overrightarrow{E_y}$, where depending of the value amplitudes, $\mathrm{E_{0x}}$ and $\mathrm{E_{0y}}$, and the phase difference ($\delta = \delta_y - \delta_x$) between these components, will represent the polarization state of the electric field $\vec{E}$. This description is reported observing to the source.

Such column vector is known as a "Jones vector":

$$\text{Jones vector} \qquad \vec{E} = \begin{pmatrix} E\cos(\theta)e^{i\delta_x} \\ E\sin(\theta)e^{i\delta_y} \end{pmatrix}. \qquad (2.4.1)$$

Where θ indicates the angle between the electric field $\vec{E}$ and one of its orthogonal components ($\overrightarrow{\mathrm{E_x}}$, $\overrightarrow{E_y}$). Therefore, the Jones vector can be written in terms of the amplitude values of the orthogonal components:

$$\vec{E} = \begin{pmatrix} \mathrm{E_{0x}} \\ \mathrm{E_{0y}} e^{i\delta} \end{pmatrix}. \qquad (2.4.2)$$

The Jones vectors also can be represented by:

$$\vec{E} = \overrightarrow{E_x} + \overrightarrow{E_y}. \qquad (2.4.3)$$

With $\overrightarrow{E_x} = \mathrm{E_{0x}}\, e^{i(\omega t - kz)}\, \widehat{e_x}$ and $\overrightarrow{E_y} = \mathrm{E_{0y}}\, e^{i(\omega t - kz + \delta)}\, \widehat{e_y}$; where $\overrightarrow{E_x}$ and $\overrightarrow{E_y}$ travel along a same direction, and for simplicity the vectorial components are in the direction S associated to the propagation direction (along the z axis, according to the Fig. (5)), which is perpendicular to the electric field.

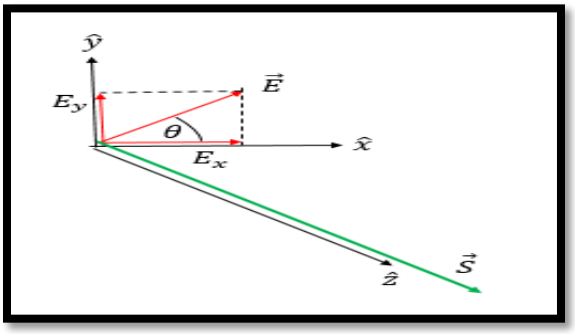

Figure 5. Vector of the electric field $\vec{E}$ to an angle θ with respect to the x axis, where its respective orthogonal components $\overrightarrow{E_x}$ and $\overrightarrow{E_y}$ are traveling along the optical z axis.

Therefore, each polarization state has associated a single Jones vector, which can be represented by:

$$\hat{E} = \begin{pmatrix} 1 \\ 0 \end{pmatrix} \quad \rightarrow \quad (\mathrm{p}) - \text{linearly polarized state}$$

$$\hat{E} = \begin{pmatrix} 0 \\ 1 \end{pmatrix} \quad \rightarrow \quad (\mathrm{s}) - \text{linearly polarized state}$$

$$\hat{E} = \frac{1}{\sqrt{2}} \begin{pmatrix} 1 \\ 1 \end{pmatrix} \quad \rightarrow \quad (+45 \text{ degrees}) - \text{linearly polarized state}$$

$$\hat{E} = \frac{1}{\sqrt{2}} \begin{pmatrix} 1 \\ -1 \end{pmatrix} \quad \rightarrow \quad (-45 \text{ degrees}) - \text{linearly polarized state}$$

$$\hat{E} = \begin{pmatrix} \cos(\theta) \\ \sin(\theta) \end{pmatrix} \quad \rightarrow \quad (\theta) - \text{linearly polarized state}$$

Where θ indicates any angle between the electric field $\vec{E}$ and its components $\overrightarrow{\mathrm{E_x}}$.

$$\hat{E} = \frac{1}{\sqrt{2}} \begin{pmatrix} 1 \\ i \end{pmatrix} \quad \rightarrow \quad (\mathrm{R}) - \text{Circularly right} - \text{hand polarized state}$$

$\hat{E} = \frac{1}{\sqrt{2}} \begin{pmatrix} 1 \\ -i \end{pmatrix}$ → (L) − Circularly left − hand polarized state

$\vec{E} = \begin{pmatrix} \mathrm{E_{0y}} \\ e^{\pm i\delta}\,\mathrm{E_{0x}} \end{pmatrix}$ → Elliptically polarized state

$With\ \hat{E} = \frac{\vec{E}}{|\vec{E}|}$.

Although the traced path end of the electric field $\vec{E}$ is well defined, the polarization state could be changed depending on the interaction of light with matter (optical elements, material samples or simply an object that polarizing the incident beam), and therefore each object will have an associated matrix, and it is commonly known as "Jones Matrix":

Jones matrix $$J = \begin{pmatrix} J_{xx} & J_{xy} \\ J_{yx} & J_{yy} \end{pmatrix}. \quad (2.4.4)$$

Which depending of its values (J_{xx}, J_{xy}, J_{yx} and J_{yy}), will be the change in the polarization state of the light beam that impinge on the object, and this physical behavior can be represented by:

$$\hat{E}^o = J\hat{E}^i\,. \quad (2.4.5)$$

Where $\hat{E}^i$ and $\hat{E}^o$ is the polarization state represents by the Jones notation, before and after passing through the object, and J represent the Jones matrix of any object. This assumption is done considering a linear response to light.

Stokes matrix formalism (second formalism)

In this formalism the polarization states of the light, which may be totally polarized, partially polarized, or totally unpolarized and these are represented as column vectors of dimensions 4×1, commonly known as "Stokes vector" S. The Stokes vector are also related to observable quantities which are:

$$S = \begin{pmatrix} I_p + I_s \\ I_p - I_s \\ I_+ - I_- \\ I_R - I_L \end{pmatrix}. \quad (2.4.6)$$

Where I_p, I_s, I_+ and I_- represent the intensities of the linearly polarized electric field to 0, 90, 45 and -45 degrees, respectively, and I_R and I_L represent the intensities of the circularly polarized electric field at clockwise and counter-clockwise sense, respectively (observing to the source direction). Besides, these intensities also can be represented in function of the amplitudes of the orthogonal components of the electric field $\vec{E}$ (E_x and E_y) and their phase difference, so the Stokes vector can be represented as:

$$S = \begin{pmatrix} E_x E_x{}^* + E_y E_y{}^* \\ E_x E_x{}^* - E_y E_y{}^* \\ E_x E_y{}^* + E_y E_x{}^* \\ i\,(E_x E_y{}^* - E_y E_x{}^*) \end{pmatrix}. \qquad (2.4.7)$$

Therefore, each polarization state has associated a single Stokes vector, which can be represented by:

$$S = \begin{pmatrix} 1 \\ 1 \\ 0 \\ 0 \end{pmatrix} \qquad \rightarrow \quad (\mathrm{p}) - \text{linearly polarized state}$$

With $\mathrm{E_{0x}}$ normalized to unity, and therefore $|\mathrm{E_{0x}}|^2 = 1$

$$S = \begin{pmatrix} 1 \\ -1 \\ 0 \\ 0 \end{pmatrix} \qquad \rightarrow \quad (\mathrm{s}) - \text{linearly polarized state}$$

With $\mathrm{E_{0y}}$ normalized to unity, and $\left|\mathrm{E_{0y}}\right|^2 = 1$

$$S = 2\begin{pmatrix} 1 \\ 0 \\ 1 \\ 0 \end{pmatrix} \qquad \rightarrow \quad (+45 \text{ degrees}) - \text{linearly polarized state}$$

With $\mathrm{E_{0x}}$ normalized to unity, and $|\mathrm{E_{0x}}|^2 = 1$

$$S = 2\begin{pmatrix} 1 \\ 0 \\ -1 \\ 0 \end{pmatrix} \qquad \rightarrow \quad (-45 \text{ degrees}) - \text{linearly polarized state}$$

With $\mathrm{E_{0y}}$ normalized to unity, and $\left|\mathrm{E_{0y}}\right|^2 = 1$

$$S = \begin{pmatrix} 1 \\ \cos(2\theta) \\ \sin(2\theta) \\ 0 \end{pmatrix} \qquad \rightarrow \quad (\theta) - \text{linearly polarized state}$$

With E normalized to unity, $|\mathrm{E}|^2 = 1$, where $\vec{E} = \overrightarrow{E_x} + \overrightarrow{E_y}$ and θ is the angle between the electric field $\vec{E}$ and its component $\overrightarrow{E_y}$.

$$S = 2\begin{pmatrix} 1 \\ 0 \\ 0 \\ 1 \end{pmatrix} \qquad \rightarrow \quad (\mathrm{R}) - \text{Circularly right} - \text{hand polarized state}$$

With $\mathrm{E_{0x}}$ normalized to unity, $|\mathrm{E_{0x}}|^2 = 1$

$$S = 2\begin{pmatrix} 1 \\ 0 \\ 0 \\ -1 \end{pmatrix} \quad \rightarrow \quad \text{(L)} - \text{Circularly left} - \text{hand polarized state}$$

With $\mathrm{E_{0x}}$ normalized to unity, $|\mathrm{E_{0x}}|^2 = 1$

$$S = \begin{pmatrix} \mathrm{E_{0x}}^2 + \mathrm{E_{0y}}^2 \\ \mathrm{E_{0x}}^2 - \mathrm{E_{0y}}^2 \\ 2\mathrm{E_{0x}}\mathrm{E_{0y}}\cos(\delta) \\ 2\mathrm{E_{0x}}\mathrm{E_{0y}}\sin(\delta) \end{pmatrix} \quad \rightarrow \quad \text{Elliptically polarized state}$$

Where $\mathrm{E_{0x}}$ and $\mathrm{E_{0y}}$ have real values, $\delta = \delta_y - \delta_x$, and $\mathrm{E_{0x}}, \mathrm{E_{0y}} \in \mathbb{R}$

$$S = \begin{pmatrix} 1 \\ 0 \\ 0 \\ 0 \end{pmatrix} \quad \rightarrow \quad \text{Unpolarized state}$$

With intensity I normalized to unity ($I = 1$)

$$S = (1 - DoP)\begin{pmatrix} 1 \\ 0 \\ 0 \\ 0 \end{pmatrix} + DoP\begin{pmatrix} 1 \\ S_1 \\ S_2 \\ S_3 \end{pmatrix} \rightarrow \quad \text{Partially polarized state}$$

With S_1, S_2 and S_3 values that represent any completely polarized state, intensity normalized to unity ($S_0 = 1$) and degree of polarization between zero and one ($1 \geq DoP \geq 0$).

If the polarization of the electric field $\vec{E}$ is known, the polarization state can be modified depending on the interaction of the light with matter, that is, according to the physical characteristics of the material medium, optical element, or object. Therefore, each object has an associated matrix, commonly known as "Mueller Matrix", which can be represented by:

Mueller matrix
$$M = \begin{pmatrix} m_{00} & m_{01} & m_{02} & m_{03} \\ m_{10} & m_{11} & m_{12} & m_{13} \\ m_{20} & m_{21} & m_{22} & m_{23} \\ m_{30} & m_{31} & m_{32} & m_{33} \end{pmatrix}. \qquad (2.4.8)$$

Depending on the values of its elements m_{ij} an incident light beam with a given polarization state will experiment a change of state given by:

$$S^o = MS^i\,. \qquad (2.4.9)$$

Where S^i and S^o are the polarization states represented by the Stokes notation, before and after passing through the object.

Chapter 3

Cylindrical vector-beams.

---

3. Cylindrical vector beams.

Electromagnetic waves are oscillatory disturbances caused by moving electric charges that transfer energy and can be able to travel through any medium or vacuum, and their existence can be demonstrated by the Maxwell's equations:

Magnetic Gauss's law $$\nabla \cdot \mu\vec{\mathrm{H}} = 0\,. \tag{3.1}$$

Electric Gauss's law $$\nabla \cdot \vec{\mathrm{E}} = \frac{\rho_q}{\varepsilon}\,. \tag{3.2}$$

Faraday's law of induction $$\nabla \times \vec{\mathrm{E}} = -\frac{\partial \mu\vec{\mathrm{H}}}{\partial t}\,. \tag{3.3}$$

Ampère's law $$\nabla \times \mu\vec{\mathrm{H}} = \mu\left(\sigma\vec{\mathrm{E}} + \varepsilon\frac{\partial\vec{\mathrm{E}}}{\partial t}\right). \tag{3.4}$$

(Which are expressed in the international system of units "SI")

In these equations $\vec{\mathrm{H}}$ is the vector of the intensity of the magnetic field, $\vec{\mathrm{E}}$ is the electric field, and ρ_q is the electric charge density of the medium where the fields are propagated; and whose properties μ, ε and σ represent the magnetic permeability, the electrical permittivity and electric conductivity of the medium, respectively.

The physical relationships that represent the response of the linear media under the interaction with the fields are called commonly constitutive relationships:

$$\vec{\mathrm{B}} = \mu\vec{\mathrm{H}}\,. \tag{3.5}$$

$$\vec{\mathrm{D}} = \varepsilon\vec{\mathrm{E}}\,. \tag{3.6}$$

$$\vec{\mathrm{J}} = \sigma\vec{\mathrm{E}}\,. \tag{3.7}$$

(These relationships suppose an isotropic and homogeneous medium, implying that μ, ε, σ are scalars)

$\vec{\mathrm{B}}$ is the magnetic induction field, $\vec{\mathrm{D}}$ is the electric displacement field and is the responsible for the effects of free and bound charges within a medium, and $\vec{\mathrm{J}}$ is the electric current density.

On the other hand, if $\vec{\mathrm{H}}$ or $\vec{\mathrm{E}}$ are analyzed like waves that travel through a isotropic and homogeneous medium without electric charge density and electric conductivity , it is possible to know the propagation of these fields by using the wave equation:

$$\nabla^2 \psi(\mathrm{r}, t) - \frac{1}{v^2}\frac{\partial^2}{\partial t^2}\psi(\mathrm{r}, t) = 0\,. \tag{3.8}$$

Where $\psi(\mathrm{r}, t)$ is the wave function of the studied field, and whose function depends on the position vector r and the time t. Such field is propagated through a medium to speed v, which depends on the properties of said medium:

$$v = \frac{1}{\sqrt{\mu\varepsilon}}\,. \tag{3.9}$$

Therefore, if the electric field has harmonic dependence over time, the wave can be expressed mathematically as:

$$\psi(\mathrm{r}, t) = E(r)e^{-i\omega t}\,. \tag{3.10}$$

Where $E(r)$ is the amplitude of the electric field in function of the position r traveling in direction $\vec{\mathrm{k}}$, that is, the wave vector that points to the direction of propagation of the wave, whose magnitude indicated the number of times that fits the wavelength "λ" of the wave of electric field in a cycle ($k = 2\pi/\lambda$) and also represents the ratio between the angular frequency and the speed of the wave in the medium ($k = \omega/v$).

Thus, if $\psi(\mathrm{r}, t)$ is replaced in the wave equation Eq. (3.8), is obtained as result the scalar Helmholtz equation, which can be represented by:

$$(\nabla^2 + k^2)E(r) = 0\,. \tag{3.11}$$

Where this equation can be used to describe the propagation of either a linearly polarized electromagnetic wave or a single Cartesian component of an arbitrary vectorial field, and whose solution represents the spatial characteristics of wave in free space. However, when the propagation of the electric field is analyzed as a whole, this propagation can be described by the vectorial wave equation, which can be written as:

$$\nabla \times \nabla \times \vec{\psi}(\mathrm{r}, t) - k^2\vec{\psi}(\mathrm{r}, t) = 0\,. \tag{3.12}$$

The Maxwell's wave equation can have more than one solution, depending on the physical conditions of the problem, will be the kind of beam that complies with the necessary conditions to resolve the problem evaluated. In this work are studied laser beams also known as vector-beams, which are analyzed like vector-beams with axial symmetry, best

known as cylindrical vector-beams. These cylindrical vector-beams are the axially symmetric beam solution to the full vector electromagnetic wave equation and therefore also are solutions of Maxwell's equations that obey axial symmetry in both amplitude and phase, and are inside one class of spatially variant polarization, which leads a new high-NA focusing properties. These beams can be generated via different active and passive methods.

Although the cylindrical vector-beams are solutions of Maxwell's equations and so same of the scalar Helmholtz equation, these beams can have more than one mathematical expression as solution, which are known as modes, and describe mathematical solutions with different physical characteristics. For beams with paraxial propagating over the optical axis, there are two families of solutions to the scalar Helmholtz equation in the paraxial limit, which are known as Hermite–Gauss and Laguerre–Gauss family, that is, in rectangular coordinates (x, y, z) the Hermite-Gauss modes, and in cylindrical coordinates (ρ, ϕ, z) the Laguerre–Gauss modes.

3.1. Introduction

The azimuthally symmetric Gaussian-beam appears as the lowest-order member of each solution belonging the family of scalar Helmholtz equation.

Therefore, if one assumes a scalar electric field $E = f(\rho, \phi, z)e^{i(kz-\omega t)}$, which propagates along the optical z-axis, its wavefront varies slowly $\left(\frac{\partial^2 f(\rho,\phi,z)}{\partial z^2} \approx 0\right)$, giving rise to the elementary Gaussian beam as a solution in cylindrical coordinates (ρ, ϕ, z) of the scalar Helmholtz equation in the paraxial limit and with amplitude $f(\rho, \phi, z)$ [8], which satisfies the next equation:

$$\frac{1}{\rho}\frac{\partial}{\partial \rho}\left(\rho \frac{\partial f(\rho,\phi,z)}{\partial \rho}\right) + \frac{1}{\rho^2}\frac{\partial^2 f}{\partial \phi^2} + 2ik\frac{\partial f(\rho,\phi,z)}{\partial z} = 0\,. \tag{3.1.1}$$

Where k and ω are the wavenumber and the circular frequency, respectively. On the other hand, if the elementary Gaussian mode has azimuthal symmetry, that is, it is not dependent on ϕ, the Eq. (3.1.1) simplifies to [8]:

$$\frac{1}{\rho}\frac{\partial}{\partial \rho}\left(\rho \frac{\partial f(\rho,z)}{\partial \rho}\right) + 2ik\frac{\partial f(\rho,z)}{\partial z} = 0\,. \tag{3.1.2}$$

The solution to the Eq. (3.1.2), is given by:

$$f(\rho,z) = \frac{w_0}{w(z)}e^{-i\Phi(z)}e^{\left(\frac{-\rho^2}{{w_0}^2\left(1+\frac{iz}{L}\right)}\right)}\,. \tag{3.1.3}$$

Where $\mathrm{L} = \mathrm{k}{\mathrm{w}_0}^2/2$, is the Rayleigh length, $\mathrm{w(z)} = \mathrm{w}_0\sqrt{1+\left(\frac{\mathrm{z}}{\mathrm{L}}\right)^2}$, and $\Phi(\mathrm{z}) = \arctan\left(\frac{\mathrm{z}}{\mathrm{L}}\right)$, w_0 is the beam waist at $\mathrm{z} = \mathrm{L}$, where there is a high concentration of energy Fig. (1).

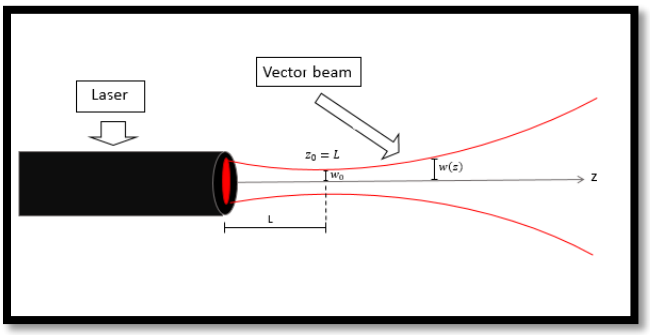

Figure 1. Vector beam with its main parameters.

3.2. Mathematical description of cylindrical vector beams

According to the previous statement, there are two types of polarization, where the non-conventional varies spatially, that is, the electric field vectors in the beam cross-section at an given instant, do not point at the same direction and sense.

Thus, the cylindrical vector beams have transversal characteristics as spatially variant polarization and are axially symmetric, which are important properties of radiation. For a vector-beam within the paraxial approximation along the z-axis, the proposed solution of the Eq. (3.11) in Cartesian coordinates can be represented by:

$$E(x,y,z,t) = A(x,y,z)e^{i(kz-\omega t)}\,. \tag{3.1.4}$$

Inserting the Eq. (3.1.4) into the Eq. (3.12) and considering the paraxial approximation appropriate, the Hermite-Gauss solution modes (HG) is obtained by the separation of variables method, where this solution represents the amplitude distribution $A(x,y,z)$ of the field $E(x,y,z,t=0)$, which can be represented by [19]:

$$A(x,y,z) = E_0 H_m\left(\sqrt{2}\frac{x}{w(z)}\right)H_n\left(\sqrt{2}\frac{y}{w(z)}\right)\frac{w_0}{w(z)}e^{-i\Phi(z,m,n)}e^{\left(-\frac{x^2+y^2}{{w_0}^2\left(1+\frac{iz}{L}\right)}\right)}\,. \tag{3.1.5}$$

Where $H_m(\cdots)$ and $H_n(\cdots)$ represent the probabilistic Hermite polynomials of m and n degrees respectively, which are solutions of the differential equation [20]:

$$\frac{d^2}{du^2}\,q(u) - 2u\,\frac{d}{du}\,q(u) + 2v\,q(u) = 0\,. \tag{3.1.6}$$

The general solution of Eq. (3.1.6) can be written as [20]:

$$H_v(u) = (-1)^v e^{u^2}\frac{d^v}{du^v}\left(e^{-u^2}\right). \tag{3.1.7}$$

Where E_0 is a constant electric field amplitude, $w(z)$ is the beam waist at a distance z, w_0 is the beam waist to the Rayleigh length $\mathrm{L} = \mathrm{k}{w_0}^2/2$, and $\Phi(z,m,n) = (m+n+1)\ arc\tan\left(\frac{z}{L}\right)$ is the Gouy phase shift.

Similarly, for a vector-beam within the paraxial approximation, the proposed solution of the Eq. (3.11) in Cylindrical coordinates can be represented by [19]:

$$E(\rho,\phi\ ,z,t) = A(\rho,\phi,z)e^{i(kz-\omega t)}\ . \tag{3.1.8}$$

Inserting Eq. (3.1.8) into Eq. (3.11) the Laguerre-Gauss solution modes (LG) is obtained by the separation of variables method, [19]:

$$A(\rho,\phi,z) = E_0\left(\sqrt{2}\frac{r}{\omega}\right)^l L_p^l\left(2\frac{r^2}{\omega^2}\right)\frac{w_0}{w(z)}\ e^{-i\Phi(z,p,l)}e^{\left(-\frac{r^2}{{w_0}^2\left(1+\frac{iz}{L}\right)}\right)}e^{il\phi}\ . \tag{3.1.9}$$

With $e^{il\phi}$ as phase term type vortex and $L_p^l(\cdots)$ representing the generalized Laguerre polynomials of p order, which are solutions to the differential equation [20]:

$$u\ \frac{d^2}{du^2}\ q(u) + (l+1-u)\frac{d}{du}\ q(u) + p\ q(u) = 0. \tag{3.1.10}$$

The Rodrigues formula of Laguerre polynomials is [20]:

$$L_p^l(u) = \frac{1}{n!}\frac{e^u}{u^l}\frac{d^p}{du^p}\left(\frac{e^{p+l}}{e^u}\right). \tag{3.1.11}$$

$\Phi(z,p,l) = (2p+l+1)\ arc\tan\left(\frac{z}{L}\right)$ is the Gouy phase shift.

An alternative solution that satisfies Eq. (3.11) also in Cylindrical coordinates, is known as the Bessel-Gauss beam solution, which represents a beam with azimuthal symmetry (it is not dependent of the ϕ-coordinate) [19]:

$$A(\rho,z) = E_0\ \frac{w_0}{w(z)}\ \ e^{-i\Phi(z)}e^{\left(-\frac{r^2}{{w_0}^2\left(1+\frac{iz}{L}\right)}\right)}J_0\left(\frac{\beta\rho}{1+i\frac{z}{L}}\right)e^{\left(-\frac{\beta^2 z}{2k\left(1+i\frac{z}{L}\right)}\right)}. \tag{3.1.12}$$

Where β is a constant scale parameter and $J_0(\cdots)$ is the zeroth-order Bessel function of the first kind; similarly, when $\beta = 0$, the above solution is reduced to the elementary Gaussian beam solution. On the other hand, the Bessel-Gauss beam is a diffraction-free beam that carries a finite power and can be realized experimentally. When the parameter β is very small, the Bessel-Gauss vector-beam at the waist ($z = L$) can be approximated by [19]:

$$\vec{E}(r,z) = C\ re^{-\frac{1}{w(z)}r^2}\vec{e}_{r,\phi}\ . \tag{3.1.13}$$

Where C is an amplitude constant and $\hat{e}_{r,\phi}$ is an unit vector in the r or ϕ direction, and this amplitude profile is equal to the LG_{01} mode but without the vortex phase term $e^{il\phi}$ [19].

Therefore, if a vectorial electric field is considered for the vectorial wave equation Eq. (3.12) in Cylindrical coordinates, the solution for a axially symmetric field $\vec{E}$ that travels along the z-axis with an oscillation direction on the ϕ-axis, it can be written as [19]:

$$\vec{E}(\rho,z) = A(\rho,z)\, e^{i(kz-\omega t)}\, \vec{e}_{\phi}\,. \tag{3.1.14}$$

Where $A(\rho,z)$ and $\vec{e}_{\phi}$, are the amplitude and the oscillation direction of the vectorial azimuthally symmetric field $\vec{E}(\rho,z)$, respectively.

Then, inserting the Eq. (3.1.13) into the Eq. (3.12) within the appropriate paraxial limit, [8]:

$$\frac{1}{\rho}\frac{\partial}{\partial\rho}\left(\rho\frac{\partial}{\partial x}\,A(\rho,z)\right) - \frac{1}{\rho^2}\,A(\rho,z) + 2ik\,\frac{\partial}{\partial z}\,A(\rho,z)\,. \tag{3.1.15}$$

The solution for the above equation can be represented by [8]:

$$A(\rho,z) = E_0\,\frac{w_0}{w(z)}e^{-i\Phi(z)}e^{\left(\frac{-\rho^2}{{w_0}^2\left(1+\frac{iz}{L}\right)}\right)}J_1\left(\frac{\beta\rho}{1+i\frac{z}{L}}\right)e^{\left(-i\frac{\beta^2 z}{2k\left(1+i\frac{z}{L}\right)}\right)}. \tag{3.1.16}$$

Where $A(\rho,z)$ is the amplitude of the electric field with oscillation direction on the ϕ-axis, this means that $\vec{E}(\rho,z)$ has associated an azimuthal polarization.

An electric field has associated a magnetic field perpendicular to it, so given an azimuthal electric field, there is a radially polarized magnetic field.

In the same way, if one has an azimuthally polarized magnetic field, there is a radially polarized electric field associated to it, so that an azimuthally polarized magnetic field can be represented by [19]:

$$\vec{H}(\rho,z) = -B(\rho,z)\, e^{i(kz-\omega t)}\, \vec{e}_{\phi}\,. \tag{3.1.17}$$

Where $B(\rho,z)$ is the amplitude of the magnetic field $\vec{H}(\rho,z)$, and whose amplitude $B(\rho,z)$ can be written as [19]:

$$B(\rho,z) = H_0\,\frac{w_0}{w(z)}e^{-i\Phi(z)}e^{\left(\frac{-\rho^2}{{w_0}^2\left(1+\frac{iz}{L}\right)}\right)}J_1\left(\frac{\beta\rho}{1+i\frac{z}{L}}\right)e^{\left(-i\frac{\beta^2 z}{2k\left(1+i\frac{z}{L}\right)}\right)}. \tag{3.1.18}$$

With H_0 as a constant magnetic field amplitude.

Thus, for the magnetic field $\vec{H}(\rho, z)$, the corresponding electric field has a radial polarization, that is, is an electric radially polarized field. Therefore, the linear superposition of the radially and azimuthally polarized fields can generate cylindrical vector-beams.

Chapter 4

Generating focal fields using optical vector fields

---

4. Generating focal fields using optical vector fields

As previously mentioned, the cylindrical vector-beams are vector-beams with axial symmetry in both amplitude and phase, in other words, vector-beams with axial symmetry in polarization, so a possible polarization mode for these vector-beams is the mode with radial polarization, which is the main characteristic for generating a longitudinally polarized beams with sub-wavelength waist and flat intensity profile, that is, an axial electric field component generated by focusing a radially polarized beam, where this component also is known as optical needle and it is formed within the depth of focus (DOF) of a specific optical system.

Nowadays, a longitudinally polarized beam can be generated by using very sophisticated methods, which contain optical elements and light sources, whose characteristics can be modified in order to obtain a narrow and long beam. At the same time, these methods allow to enhance a very long DOF, where the beam propagates without divergence. Therefore, the most commonly used optical elements are the objective lenses (by varying its numerical aperture), mirrors (by varying its geometrical form) and diffractive optical elements (by varying its geometry and manufacturing materials).

4.1. Diffractive optical element, DOE

Before beginning to define the diffraction phenomenon, it will be discussed firstly the refraction phenomenon which can be defined as the bending of light rays under a change of medium.

Almost all the optical systems use refractive or reflective surfaces (optical elements like lenses, mirrors, prisms and/or films with varying thickness) and in this manner manipulate the distribution of light that arrive the system.

An optical system is a set of surfaces separating mediums with different refractive index, respectively. They can be classified into three categories: Firstly dioptric systems (formed someone by refractive surfaces), secondly catoptric systems (formed someone by reflective surfaces) and lastly catadioptric systems (formed by refractive and reflective surfaces).

Thus, these systems use a combination of lenses and mirrors in order to improve the image quality.

The diffraction phenomenon is the process by which a beam of light or other system of waves is spread out and deflected as a result of passing through a narrow aperture (an aperture less than or equal to the wavelength diameter of beam) or across an edge of opaque body, typically accompanied by interference between the waves forms produced. The study of diffraction phenomenon has a great contribution and importance in the analysis of wave propagation in the areas of physical optics and optical engineering.

Depending of the investigation area where the system is analyzed, it is possible to substitute refractive or reflective elements by diffractive optical elements “DOE”, to achieve greater efficiency. On the other hand, the single diffractive optical elements can have several focal points, generally they have much less weight and occupy less volume than the refractive or reflective elements. They may also be less expensive to manufacture and in some cases may have high optical performance, for example a wider field of view. Examples of applications of such components include optical heads for compact disks, beam shaping for lasers, grating beam-splitters, and reference elements in interferometric testing. Therefore, the diffractive optics is responsible of perform the study of functions that would be difficult or impossible to achieve with basic principles of optics by the use of DOEs.

4.2. Methods for creating specific focusing patterns

There are some methods for creating specific focusing radiation patterns in the form of an optical needle, which is an electric field distribution with extremely high longitudinal polarization purity and transverse small size, in comparison with the longitudinal field component. Such methods have been reported both theoretically and experimentally, and are grouped into four main categories:

First category

Recently, some ideas have been proposed for the implementation of longitudinal field in different areas as particle acceleration, fluorescent imaging, second-harmonic generation and Raman spectroscopy [1, 2]. Due to the importance of these fields, some methods have been suggested to enhance the longitudinal field component, but the results obtained with all of them lack enough optical efficiency and uniformity in the axial field strength. Therefore, a new method that permits the combination of very unusual properties of light in the focal region, well-known as deep of focus “DOF” and is the focus space that is found before and after of effective focal plane and limited for the paraxial focal plane and marginal focal plane respectively Fig. (1).

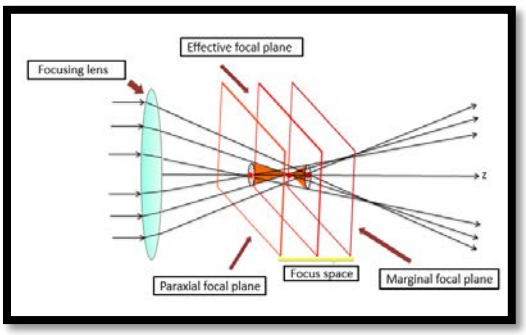

Figure 1. DOF along z axis of a focusing lens

Thus, it allows the creation of a purely longitudinal light beam with sub-diffraction beam size (0.43 λ), where the beam is non-diffracting; that is, it propagates without divergence over a long distance (4λ) in free space [1]. This is achieved with radially polarized Bessel-Gauss "BG" beams, which are one of the vector-beam with axial symmetry in amplitude solutions of the Maxwell's wave equation in the paraxial approximation, where they are focusing by a combination of a binary-phase optical element and a lens with a high capacity to concentrate light, that is, a lens with high Numerical-Aperture "NA" and It is expressed mathematically as $\mathrm{NA} = nsin(\theta_{max})$, where n is the refractive index of the medium that wrap to the lens and θ_{max} is the maximum half angle respect to the optical axis that has the lens to concentrate light. The binary-phase optical element works as a diffractive optical element "DOE", with optical elements that can have several or many different focal points simultaneously and control the distribution of intensity along the focal region "DOF" and so enhance the longitudinal field component in form of needle, where a strong longitudinally polarized light needle, with homogeneous intensity along the optical axis, long DOF, and sub-diffraction beam size can be generated, by tight focusing a radially polarized light with a high-NA lens and a DOE, Fig. (2).

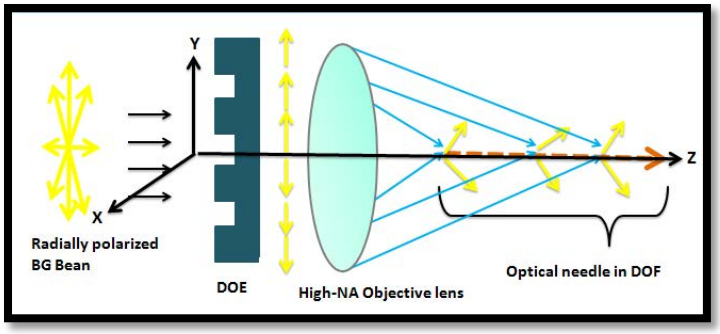

Figure 2. Optical arrangement for the generation of an optical needle.

Firstly, the incident light on the DOE is divided in two parts: cs_1 and cs_2, where the longitudinal field in the focal region is mainly dependent on the number of belts in cs_1 due to paraxial condition, but not the total number of belts in the DOE. Where the arrangement

to tight focusing the radially polarized BG beam contained a divided DOE for four rings, where the phases on each belt are 0 and π, respectively Fig. (2).

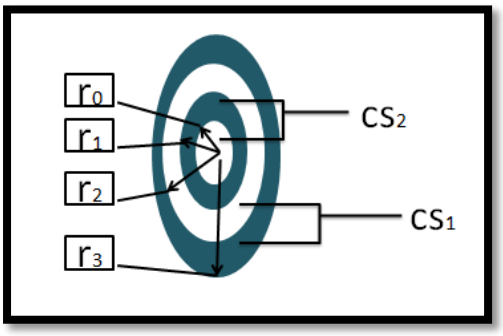

Figure 2. Four-belt DOE

According to the theory of Richards and Wolf [3, 4], when a radially polarized beam is focused by a high-NA objective lens, the field near the focal plane can be approximated by the vector Debye integral [3, 5]. Thus the radially polarized BG beam is one of the vector-beam solutions of the Maxwell's wave equation in the paraxial approximation. Therefore, the apodization function $\mathrm{I}_0(\theta)$ for a radially polarized BG beam, with the beam waist in the pupil of the focusing lens, is given by [9]:

$$\mathrm{I}_0(\theta) = \mathrm{J}_1\left(\frac{2\beta_1 \sin(\theta)}{\sin(\alpha)}\right) \mathrm{e}^{-\left(\frac{\beta_2 \sin(\theta)}{\sin(\alpha)}\right)^2} . \qquad (4.2.1)$$

Where β_1 and β_2 are taken as unity in the arrangement design, θ denotes the angle between the convergent ray and the optical axis; $\alpha = arc\sin\left(\frac{NA}{n}\right)$, with "n" as the refractive index, where to achieve an optical needle with length of 4λ along the optical axis and cross size of 0.43λ are taken values of n=1 and NA=0.95, respectively [1, 5].

Second category

The second method consists in the creation and shifting of a spherical distribution focal spot in the DOF through the focusing of radially polarized beams, in a 4π optical system.

In a 4π focusing system, radially polarized laser beams can be focused to a spherical focal spot. For many applications, e.g., for moving trapped particles or for scanning a specimen, one would like to change the position of the focal spot along the optical axis without moving lenses or laser beams. This can be achieved by modulating the phase of the input field at the pupil plane of the lens. The required phase modulation function is determined by the spherical wave expansion of the plane wave factors, when the Richards–Wolf method is applied [3,4]. The properties of the focal spot for 4π focusing with radially polarized light are presented for various apodization factors. With a focusing system satisfying the Herschel condition the focal spots are sharp and with almost-perfect spherical symmetry, obtaining equal axial and transverse resolution, achieving extremely low side-lobes [6].

When radially polarized laser beams are focused by a high-NA lens, they present unique focusing properties in comparison to linearly polarized light, a smaller focus spot and a strong axial electric field component are obtained. This result generates potential applications in many fields, e.g., electron acceleration, spectroscopy, particle trapping, and field manipulation [7]. Therefore, can be generated unusual field distributions at the focus by appropriate choice of proper amplitude or/and phase modulations on radially polarized input fields. Recently, the possibility of focusing a radially polarized beam to a sharp spherical focal spot was demonstrated theoretically for a 4π focusing system by properly choosing the input field at the pupil plane of the lens [7].Such spherical focal fields provide equal axial and transverse resolutions for confocal microscopy. Therefore, the main objective is achieve a dynamical spherical spot, that can be shifted and manipulated along the optical axis in real time.

A 4Pi focusing system consists of two confocal high-NA objective lenses illuminated by two counter-propagating radially polarized beams with the same phase, where the input fields intensity at each of the pupil planes of the lenses are denoted by $\mathrm{I_R}(\theta)$ with 0° ≤ θ ≤ 90° and $\mathrm{I_L}(\theta)$ with 0° ≤ θ ‘≤ 90° [7] measured from the propagation direction of each beam, Fig. (3).

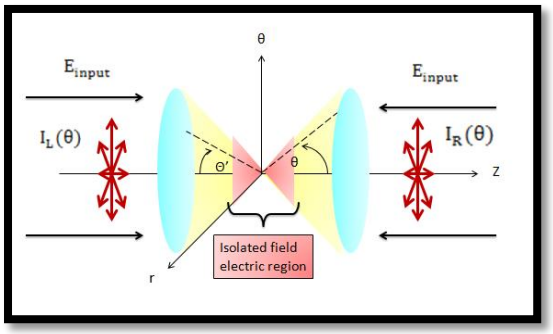

Figure 3. Arrangement of a 4Pi focusing system

These beams are focused in the focus zone of 4Pi system, where all the vectorial components of the beams are eliminated due to the fact that the counter-propagating radially polarized beams have the same phase and arrive to the center of system with opposite electric field components. Therefore is created in the DOF an isolated electric field region, where the inside of the region has not any interaction with a medium. This consequence is very important because with this method one can trap particle in the focal region and manipulate the isolated field electric region of different ways.

Thus, if the counter-propagating radially polarized beams have the same characteristics, $\mathrm{I_R}(\theta) = \mathrm{I_L}(\theta) = \mathrm{I}(\theta)$ with 0° ≤ θ ≤ 180°, the mathematical description of the interference effect can be established by using the Richards–Wolf integral, Eq. (4.2.2) and Eq. (4.2.3) [3, 4, 7, 18].

$$\mathrm{E}_r(r,z) = \int_0^{\pi} I(\theta)X(\theta)\sin(2\theta)\,J_1(krsin(\theta))e^{ikcos(\theta)z}d\theta\ . \qquad (4.2.2)$$

$$\mathrm{E}_z(r,z) = 2i\int_0^{\pi} I(\theta)X(\theta)\sin^2(\theta)\,J_0(krsin(\theta))e^{ikcos(\theta)z}d\theta\ . \qquad (4.2.3)$$

Where E_r and E_z are the radial and axial components of the electric field at an observation point P(r,z) near the focus, r, θ and z are cylindrical coordinates, $\mathrm{I}(\theta)$ is the total field intensity that arrives to each lens, X(θ) is the pupil apodization function (Eq. (4.2.4)), $\mathrm{J}_0(\mathrm{x})$ is the cylindrical Bessel function of first kind of order n, and k is the wave number [7].

$$X(\theta) = \sqrt{\cos(\theta)}\ . \qquad (4.2.4)$$

Therefore the spherical intensity distribution of the focus is maintained during dynamical movement of the focal spot along the optical axis. In conclusion, this method employs a sophisticated but very ingenious way to move a trapped particle or scan a specimen without moving the position of objective lenses [7].

Third category

The third method consists in the generation of a light needle through the modulation of radially polarized BG beam by a specific filter under a reflection system.

The light needles generated with this method are of type super-Gaussian, that is, are light needle having an intensity profile which is flat over most of the covered area of light, on the other hand, also have pure longitudinal polarization and small beam size, that is, small profile full width at half maximum "FWHM" of super-Gaussian beam (until FWHM≈0.36 λ). Where firstly, this beam impinge on a cosine synthesized filter, is an amplitude filter that modulates the incident radially polarized beam and even reshape the light needle. Where the radially polarized BG beams are modulated according to the amplitudes range that has the cosine function, achieving greater FWHM than the Gaussian profiles in the light needle. After these beams go toward a reflection system, which is a mirror with form of annular paraboloid, where all the beams impinge on the mirror of parallel form respect at optical axis, Fig. (4) [11].

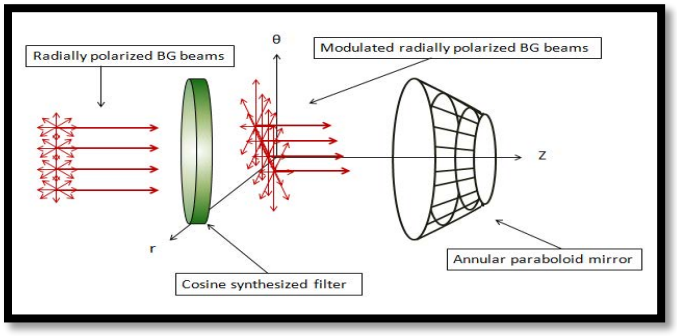

Figure 4. Optical arrangement of the third method

Since the mirror has axial symmetry, it is possible to analyze this reflection system in two dimensions, that is, like a parabolic mirror with two beams that impinge on the same mirror. Each one of the beams impinge at the lower and upper part, respectively; when the beams are reflected by the parabolic mirror, these are heading toward a specific point, where this specific point is known as focus and has the property that all the beams incident parallel at the optical axis are reflected and directed toward the focus, that is, all the beams incident of manner parallel converge in the focus of the parable.

Although all the beams incident converge in the focus and only survives the electric field components in the positive direction of Z axis, the paraxial beams and even more the beam that pass firstly for the focus are reflected in opposite direction to the electric field components of the other non-paraxial beams and parallel to the optical axis. Therefore, it is proposed to do a cross cut in the paraboloid mirror to eliminate losses of electric field, Fig. (5).

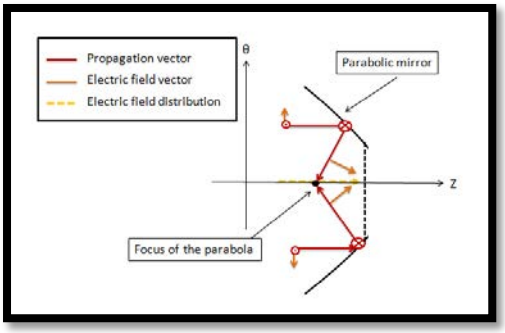

Figure 5. Cross-section of a paraboloid mirror

Thus all the beams parallel to the optical axis will generate electric field distributions along the focus of the paraboloid mirror, that is, longitudinally polarized components of the electric field in the region focal, which are described, according to the vectorial Debye-Wolf diffraction integral, Eq. (4.4.5) and Eq. (4.4.6) , as [3, 4, 12, 13, 18]:

$$\mathrm{E_r}(\mathrm{r},\mathrm{z}) = \mathrm{A_r}\int_0^{\alpha} \mathrm{I_0}(\theta)\frac{\sin(2\theta)}{1+\cos(\theta)}\mathrm{J_1}\big(\mathrm{krsin}(\theta)\big)\mathrm{e}^{-\mathrm{ikcos}(\theta)\mathrm{z}}\mathrm{d}\theta\,. \tag{4.4.5}$$

$$\mathrm{E_z}(\mathrm{r},\mathrm{z}) = -\mathrm{i2A_r}\int_0^{\alpha} \mathrm{I_0}(\theta)\frac{\sin^2(\theta)}{1+\cos(\theta)}\mathrm{J_0}\big(\mathrm{krsin}(\theta)\big)\mathrm{e}^{-\mathrm{ikcos}(\theta)\mathrm{z}}\mathrm{d}\theta\,. \tag{4.4.6}$$

Where A_r represents a constant with respect to (kf), with $k = 2\pi/\lambda$ and f being the wave number and the length between the focus and the vertex of the paraboloid, respectively; $J_{0,1}(krsin(\theta))$ are the zeroth-order and first-order Bessel functions of the first kind, respectively; α is the maximum semi-angle of the focusing light cone and (1/(1+cos(θ))) represents the apodization function of the paraboloid mirror. Since the beams are of type BG with the waist plane at the pupil plane of a paraboloid mirror, the intensity distribution with respect to θ is expressed, Eq. (4.4.7) as [1, 9, 14, 15]:

$$I_0(\theta) = e^{-\beta_0{}^2\left(\frac{\tan\left(\frac{\theta}{2}\right)}{\tan\left(\frac{\alpha}{2}\right)}\right)^2} J_1\left(2\beta_0 \frac{\tan\left(\frac{\theta}{2}\right)}{\tan\left(\frac{f}{2}\right)}\right). \quad (4.4.7)$$

Where $\beta_0 = f/w_0$ denotes the ratio of the aperture f to the beam waist w_0 and θ is the focusing angle, with $0 \leq \theta \leq \alpha$.

The obtained results reported with this method, are optical needles with consistent beam size of 0.36λ (FWHN), with electric field being purely longitudinally polarized and peak-valley intensity fluctuations within 1% for 4λ, 6λ, 8λ, and 10λ length needles [14]. The method remarkably improves the non-diffraction beam quality, compared with the sub-wavelength Gaussian light needle, which is generated by a narrow-width annular paraboloid mirror, therefore, such light beam may suit potential applications in particle acceleration, optical trapping, and microscopy [14].

Fourth category

This method consists on the generation of a diffraction-limited spherical focal spot in a 4Pi system, by combining the dipole antenna radiation pattern and the Richards–Wolf vectorial diffraction theory [2, 18].

Such method states that if a very specific input field incident on a 4π focusing system, can be generated a spherical focal spot, and said input field can be found analytically by solving the inverse problem, that is, generating a focal field with specific dimensions and by the reversing of electric field pattern radiates from a dipole array toward the focusing system, it is possible to find the input field to generating the same field in the focal region. Where the reversing due to the radiation from dipole arrays is an approach to generalized cylindrical vector beams (input field) that are focused by high NA lenses system [2].

Thus, the requested illumination to the lenses system, depend of desired focal field and its specific characteristics, so by the use of this method was reported that the input field at the pupil plane is a radially polarized field with spatial amplitude modulation. Analyzed otherwise the problem, if two radially polarized beams with spatial phase modulation and identical spherical spots with diffraction-limited size and constant distance along the optical axis, can be obtained approximately the electric field radiation pattern from a dipole array.

A spherical spot with equal three-dimensional "3D" spatial resolutions has important applications in optical microscopy, single-molecule fluorescence spectroscopy, optical data storage, particle trapping, and optical tweezers [16, 18]. In optical microscopy, a tightly focused optical field is used as a probe to investigate the sample properties within the focal volume and generate contrast for imaging [16]. For a conventional optical microscope with a single objective lens, the axial extent of the focused spot is always several times larger than the cross extent, resulting in lower longitudinal resolution. A tightly focused spherical spot with diffraction-limited size that provides equal axial and transversal resolutions is strongly desirable. Therefore to improve the axial resolution has been developed the 4Pi microscopy, which involves the use of two opposing objective lenses with high NAs and two counter-propagating beams with focused wave-fronts that had coherent interference [16].

Generally, if one use the issued electric field from a dipole antenna at the pupil plane as illumination and reverse the propagation, can be obtained a spherical spot by choosing an appropriate dipole antenna length. When the dipole antenna begins to radiate.

The field is collected and collimated by the aplanatic objective lenses, the lens pupil is calculated in conjunction with the Richards-Wolf diffraction theory. Therefore, if the angular field radiation pattern $\mathrm{R}(\theta)$ of the dipole antenna (Eq. (4.4.8)) and the respective apodization function of the pupil (Eq. (4.4.9)), one can found the input field at the lens pupil (Eq. (4.4.10)), which is an electric field radially polarized [16]:

$$\vec{\mathrm{R}}(\theta) = \mathrm{C}\frac{\left[\cos\left(\frac{\mathrm{kL}}{2}\cos(\theta)\right)-\cos\left(\frac{\mathrm{kL}}{2}\right)\right]}{\sin(\theta)}\hat{\mathrm{d}}\,. \tag{4.4.8}$$

$$\mathrm{P}(\theta) = \sqrt{\cos(\theta)}\,. \tag{4.4.9}$$

$$\vec{\mathrm{E}}_{\mathrm{i}}(\mathrm{r}) = \frac{\vec{\mathrm{R}}(\theta)}{\mathrm{P}(\theta)}\,. \tag{4.4.10}$$

Where C is a constant related with the dipole strength, k is the wavenumber, θ is the angle between the dipole antenna radiation direction and the optical z-axis, and $\hat{\mathrm{d}}$ is the unit vector of the dipole radiation field.

Note that the dipole antenna is put along of the optical axis and located in the middle of the 4Pi system, Fig. (6).

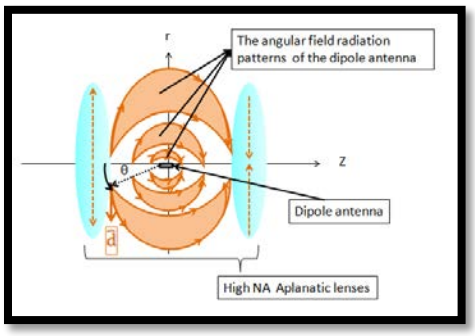

Figure 6. The angular field radiation pattern of the dipole antenna in a 4Pi system

Thus, to express the input field in the pupil plane spatial coordinates (r,φ), the projection function of the objective lens needs to be considered as an aplanatic objective lens that obeys sine condition $r = fsin(\theta)$, where r is the radial position in the pupil plane and f is the focal length of the objective lens, so the projection function from the (r, φ) space to the (θ, φ) space is the apodization function of such lens. Therefore, the field distribution propagation calculated $\vec{E}_i(r)$ as illumination in the pupil plane is reversed and so known the electric fields in the vicinity of the focal spot for radially polarization beams, by the Richards–Wolf vectorial diffraction method (Eq. (4.4.11) and Eq. (4.4.12)) [3, 4, 18]:

$$E_r(r,z) = A\int_0^{\theta_{max}} P(\theta)R(\theta)\sin(\theta)\cos(\theta)J_1(krsin(\theta))e^{-ikcos(\theta)z}d\theta\ . \qquad (4.4.11)$$

$$E_z(r,z) = iA\int_0^{\theta_{max}} P(\theta)R(\theta)\sin^2(\theta)J_0(krsin(\theta))e^{ikcos(\theta)z}d\theta\ . \qquad (4.4.12)$$

Where $E_r(r,z)$ and $E_r(r,z)$ are the radial and transversal electric field components at DOF, θ_{max} is the maximum focusing angle determined by the NA of the objective lenses and $J_{0,1}(krsin(\theta))$ are the zeroth-order and first-order Bessel functions of the first kind.

Thus, a method for 3D focus engineering was developed through reversing the electric field radiated from a dipole antenna, where adjusting the dipole antenna length to obtain a radially polarized input field with spatial amplitude modulation, are the main factors to the generation of focal fields (spherical focal spot) like an optical needle [2, 16, 17].

Chapter 5

Results

---

5. Results

In this Section are presented the results obtained from the numerical simulation derived from the generation of longitudinal polarized electric fields, which can be created by very sophisticated methods, where the results have been obtained only by numerical simulations.

5.1. Numerical simulation

A longitudinally polarized field, is a vectorial field where all the vectors associated to the points of the field region, point at the same direction of propagation of the said field. When this field is generated in the focal plane of an optical system, that is, within the depth of field "DOF", and field formed in the DOF is named focal field "FF". Therefore, if the FF has homogeneous intensity distributions along the DOF and subwavelength waist, then an optical needle is obtained. Many applications have been reported about the focusing of radially polarized vector beams to the creation of a longitudinally polarized non-diffraction beam, that is, creating an optical needle.

Therefore, to the creation of an optical needle, firstly were simulated two light source (Bessel-Gauss beam and an uniform line source), which have an electric field with radial polarization, where this property of the electric field is very important for the generation of an optical needle with longitudinal polarization, that is, longitudinally polarized non-diffracting beam over its own extension.

Thus, the field pattern radiated (Fig. (1)) from a ULS (uniform line source) is given by [10]:

$$\vec{F}(\theta) = C\sin(\theta)\frac{\sin\left[\left(\frac{kL}{2}\right)\cos(\theta)\right]}{\left(\frac{kL}{2}\right)\cos(\theta)}\vec{e}_{\theta} \ . \qquad (5.1.1)$$

(The overhead equation was deducted by using physical and mathematical arguments, which are described in the A-Appendix)

Where $C = -i\omega\mu_0 I_0 L e^{i(kr-\omega t)}/(4\pi r)$,which is normalized to 1 for convenience of computing, L and I_0 represent the length and the constant current of the ULS, respectively, which will be centered at the focus of the lens that focuses the field radiated and along the optical axis of the focusing system, ω and μ_0 are the angular frequency and the magnetic permeability in vacuum, respectively, k and r denotes the wave number and focal length of the focusing lens, respectively, θ is the angle between the radiation direction of the SLU and the optical axis of the focusing system, and $\vec{e}_\theta$ is the unit vector of the field radiated from the ULS.

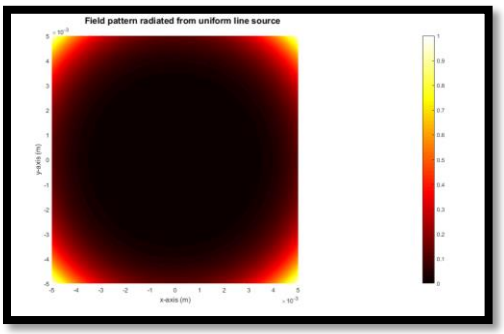

Figure 1. Cross-section of the field pattern radiated from a uniform line source of length (λ=1) in the xy-plane.

In a similar way, a Bessel-Gauss beam is a possible solution in cylindrical coordinates (r, ϕ, z) of the paraxial wave equation for an electric field with radial polarization, whose ϕ-symmetrical amplitude (Fig. (2)) can be represented by [19]:

$$U(r, z = 0) = A_0\, e^{-\frac{r^2}{{\omega_0}^2}} J_0(\beta r). \qquad (5.1.2)$$

Where A_0 is a constant parameter normalized to 1, β is the projection of the mean wave-vector of a Gaussian beam on the $z = 0$ plane, and k and ω_0 are the wavenumber and beam waist to a length equal to the Rayleigh range, respectively.

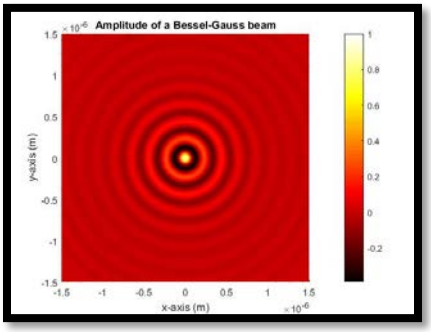

Figure 2. Amplitude of cross-section (xy-plane) associated to a Bessel-Gaussian beam, which is at $z=0$ of the optical axis.

The amplitude of Eq. (5.1.2) is composed of the propagation factor of a plane wave multiplied by a Bessel function of the first kind, of first-order, and the amplitude factor of the elementary Gaussian beam (Fig. (3)), whose amplitude can be written mathematically as [8]:

$$f(r,z) = \frac{w_0}{w(z)} e^{-i\Phi(z)} e^{\left(\frac{-r^2}{{w_0}^2\left(1+\frac{iz}{L}\right)}\right)}. \qquad (5.1.3)$$

Where $L = kw_0{}^2/2$ is the length in the Rayleigh range, $w(z) = w_0\sqrt{1+\left(\frac{z}{L}\right)^2}$, and $\Phi(z) = \arctan\left(\frac{z}{L}\right)$, w_0 is the beam waist to a length $z = L$.

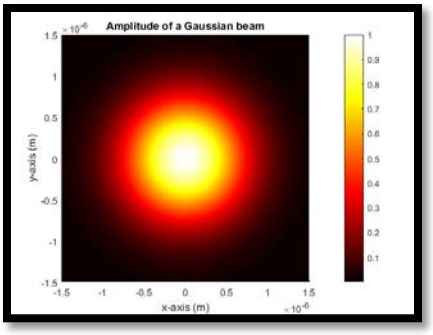

Figure 3. Cross-section (xy-plane) of the amplitude of a Gaussian beam, which is to $z=0$ of the optical axis.

Thus, in order to know the intensity distribution of the electric field along the DOF (depth of field) of a lens, both the uniform line sources and the Bessel-Gaussian beam were focused in different optical systems, where the said distribution was evaluated by the Richards-Wolf vectorial diffraction integrals [3,4]:

$$E_r(r,z) = \int_0^{\theta_{max}} E^i(\theta)P(\theta)\sin(2\theta)J_1(kr\sin(\theta))e^{ikzcos(\theta)}d\theta\,. \qquad (5.1.4)$$

$$E_z(r,z) = i2\int_0^{\theta_{max}} E^i(\theta)P(\theta)\sin^2(\theta)J_0(kr\sin(\theta))e^{ikzcos(\theta)}d\theta. \qquad (5.1.5)$$

Where $E_r(r,z)$ and $E_z(r,z)$ are the radial and the longitudinal field components at an observation point (r,z), respectively; $E^i(\theta)$ is the amplitude distribution function of the light source, $P(\theta)$ the apodization function of the optical element illuminated by the source, and θ the integration variable, which represents the angle between the optical z axis and

the r coordinate at the optical element. For both light sources, a high-NA aplanatic objective lens is used as optical element, which has an apodization function $P(\theta) = \sqrt{\cos(\theta)}$ and a maximum acceptance half-angle denoted as "θ_{max}".

Therefore, if the radial and longitudinal field components are known, it is possible to describe the intensity distribution and the longitudinally polarized beam profile along the DOF, so the intensity "I" at each observation point (r, z) can be calculated by:

$$I = |E_r(r,z)|^2 + |E_z(r,z)|^2 \,. \qquad (5.1.6)$$

Consequently, for the first light source (uniform linear source, ULS), the electric field pattern is radiated in a 4pi focused system, which is composed of two aplanatic objective lenses, each with NA=1. In order to obtain a longitudinally polarized beam, the electric field pattern is radiated and focused with a phase difference of 180 degrees ($\Delta\varphi = \pi$) between the electric fields, that is, the 4pi system is illuminated by two counter-propagating radially polarized beams with a relative π phase shift. Thus, under these conditions the longitudinally polarized beam profile Fig. (4) is flat over most of the covered area with intensity, that is, a flat-top longitudinally polarized beam; this beam is not diffracted along a distance, that is, it is a non-diffracting beam on its own extent or FWHM (full width at half maximum), where this represents the optical needle length, which depends of the size L of the uniform linear source.

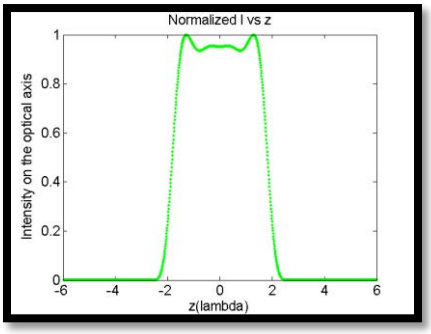

(a) Flat-top beam with 3.25λ FWHM

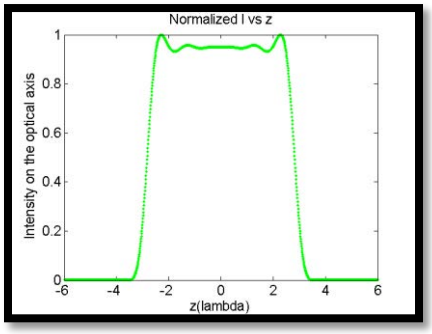

(b) Flat-top beam with 5.25 λ FWHM

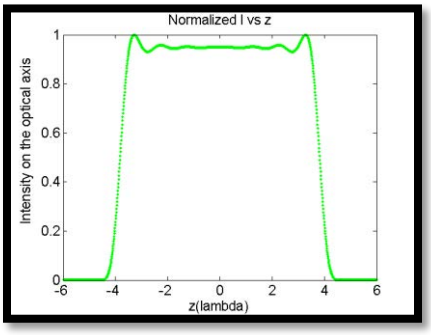

(c) Flat-top beam with 7.23λ FWHM

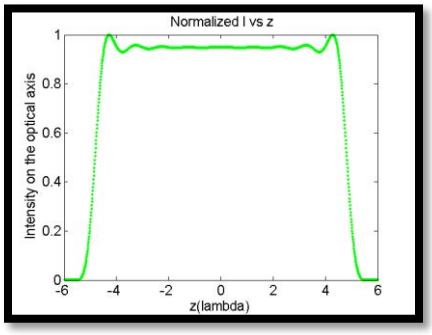

(d) Flat-top beam with 9.24λ FWHM

Figure 4. Flat-top beams with specific FWHM generated by a uniform linear source with length (a) 4λ, (b) 6λ, (c) 8λ, and (d) 10λ, respectively. B-Appendix.

Other important parameter associated to the optical needle, is its diameter, that is, the longitudinally polarized beam waist , which has a sub-wavelength size Fig. (5) and it does not change along the FWHM of the flat-top beam, where its waist w does not depend on the size L of the ULS.

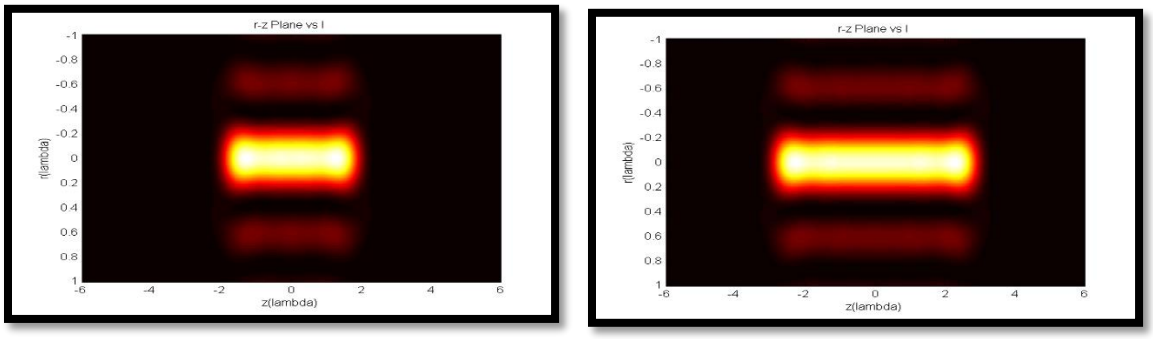

a) Optical needle with 3.25λ FWHM

b) Optical needle with 5.25λ FWHM

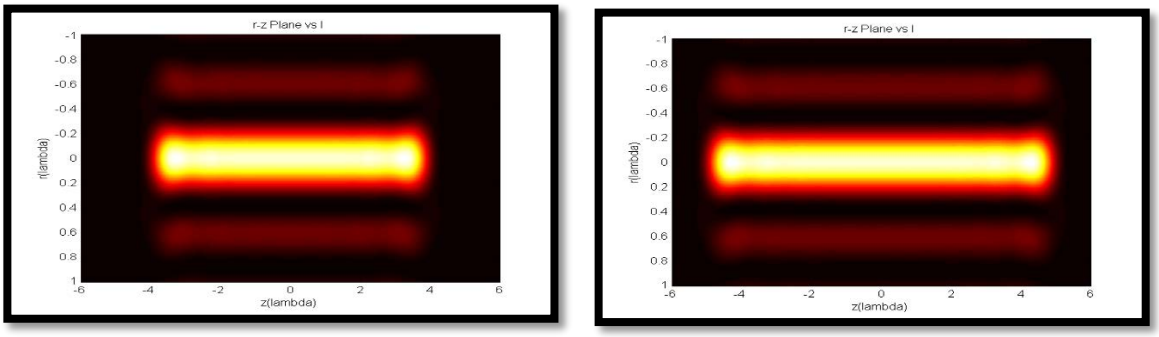

c) Optical needle with 7.23λ FWHM

d) Optical needle with 9.24λ FWHM

Figure 5. Different FWHM and equal waist (0.36λ) optical needles, which are generated by a) 4λ-, b) 6λ-, c) 8λ and d) 10λ-length uniform linear sources, respectively. C-Appendix.

Similarly, the second light source (a Bessel-Gaussian beam with radial polarization), it is focused in an aplanatic objective lens with a NA=0.95 to obtain a longitudinally polarized beam with Gaussian profile Fig. 6(a), and in order to achieve a longitudinally polarized beam with flat profile Fig. 6(b), was added a DOE (Diffractive Optical Element) with five concentric belts.

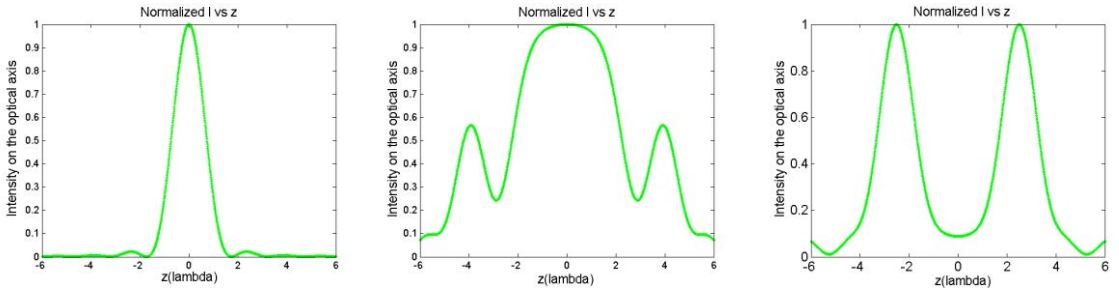

(a) Gaussian profile (b) Super-Gaussian profile (c) Two semi-Gaussian Profiles

Figure 6. A longitudinally polarized beam profile generated by (a) an aplanatic lens, (b) a hybrid lens with five equally spaced belts, and (c) a hybrid lens with five differently spaced belts, respectively. D-Appendix.

Where these DOEs are simulated both with equal and different spacing between each belt Fig. 7(a) and Fig. 7(b), respectively, and whose phase shift $\Delta\varphi$ between a belt and another of 0 and π radians, respectively; which means that the radially polarized Bessel-Gaussian beam firstly impinge on the DOE and then it is focused by the aplanatic lens, where to the set of a lens with a DOE, it will be called "hybrid lens".

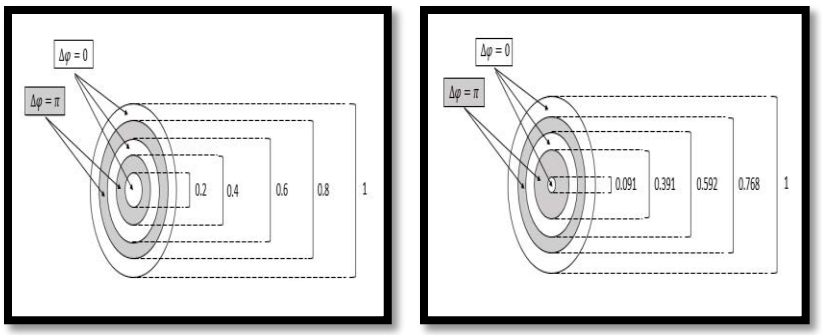

(a) DOE with five equally spaced belts (b) DOE with five differently spaced belts

Figure 7. DOE with equal and different spacing between each belts, whose relative diameters of each belt are (a) 0.2, 0.4, 0.6, 0.8 and 1, and (b) 0.091, 0.391, 0.592, 0.768 and 1, respectively.

Fig. (8) shows the geometry associated to a DOE with two concentric belts and fig. (9) shows the profiles generated numerically using an aplanatic lens with NA=0.95

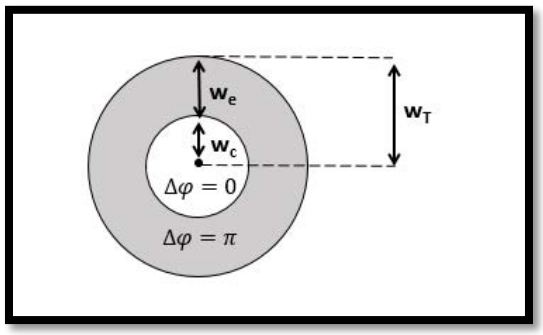

Figure 8. DOE with two concentric belts

Where this DOE was chosen with two different specifications, which are based on the values of the central and exterior widths, w_c and w_e, that is, the ratio r between the width of the center belt w_c and the width of the two belts is w_T (r= w_c / w_T).

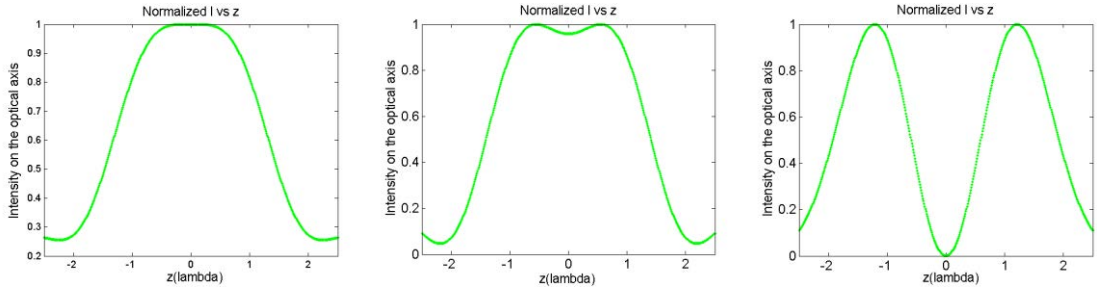

(a) Super-Gaussian profile (b) Semi-super-Gaussian profile (c) Two Gaussian Profiles

Figure 9. A longitudinally Bessel-Gaussian beam profile generated by a hybrid lens with two-belts DOE, whose ratio r are (a) 26.392/64, (b) 32/64, and (c) 46/64, respectively. E-Appendix.

Whose DOEs used to generate the profiles of the Fig. (9) are shown below.

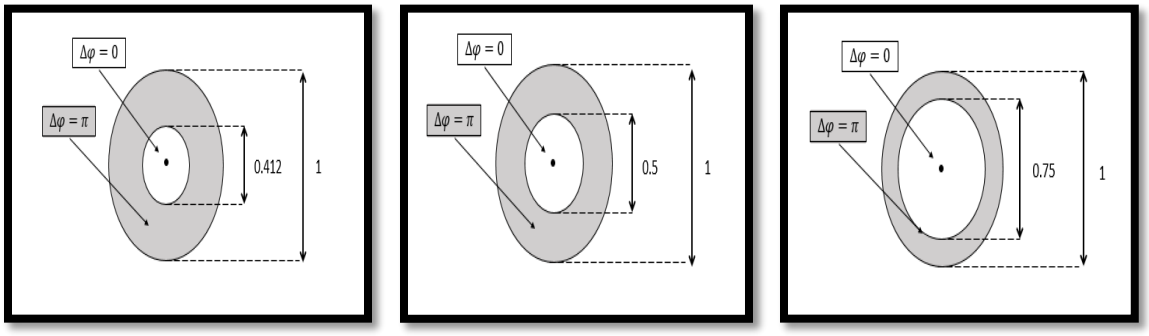

(a) Two-belts DOE with optimized parameters (b) DOE with two belts of equal width (c) DOE with two belts of different width

Figure 10. Two-belts DOEs with ratio r of (a) 26.392/64, (b) 32/64, and (c) 46/64, respectively.

Thus, when the five-belts-DOE have a different spacing between each belt, the longitudinally polarized beam profile will be flat over most of the covered area with intensity and at the same time, the beam will be non-diffractive along a distance, that is, along its own FWHM (4λ) and it represents the optical needle length, which depends of the spacing between each belt of the DOE.

Therefore, when the beam is non-diffractive, it propagates without divergence over its FWHM, implying that the beam will have a constant waist, which is of sub-wavelength size; on the other hand, the FWHM and the beam waist are parameters that depend of the characteristics of the DOE, that is, of its belts number and spacing between each one.

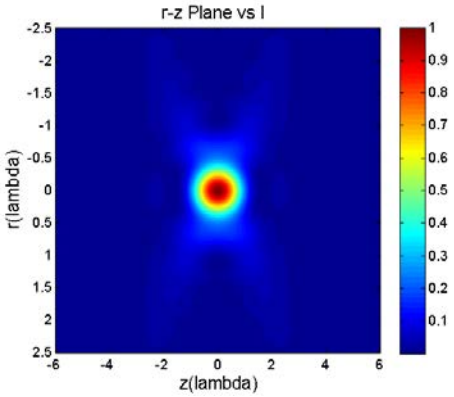

(a) Optical needle generated by only an aplanatic lens

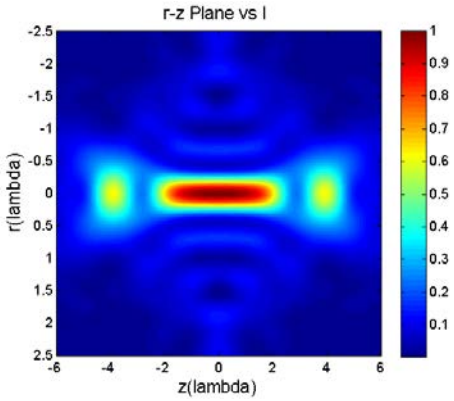

(b) Optical needle generated by hybrid lens with five differently spaced belts

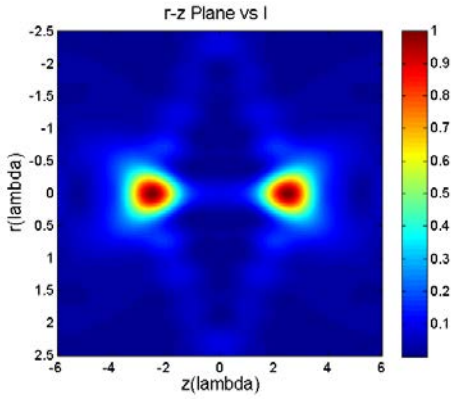

(c) Optical needles generated by hybrid lens with five equally spaced belts

Figure 11. Beams with FWHM of (a) 1.4λ and variable waist (b) 4.4λ and 0.44 λ constant waist, and (c) 1.67λ and variable waist (both), respectively (the mentioned waists are taken with respect to their own FWHM). F-Appendix.

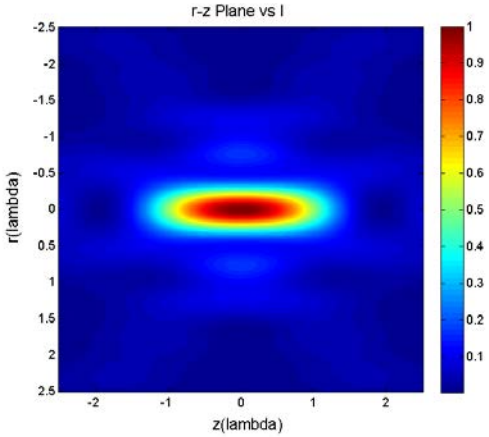

(a) Optical needle generated by hybrid lens with two belts and r=26.392/64

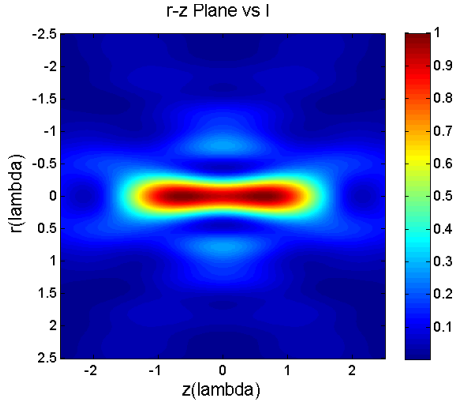

(b) Optical needle generated by hybrid lens with two equally spaced belts

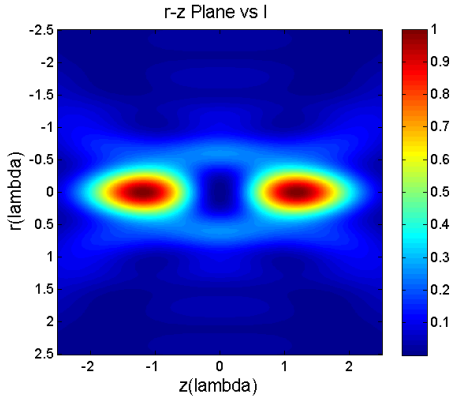

(c) Optical needle generated by hybrid lens with two belts and r=46/64

Figure 12. Beams with FWHM of (a) 2.5λ and 0.74 λ constant waist, (b) 2.72λ and variable waist, and (c) 1.75λ and variable waist (both, respectively (The mentioned waists are taken with respect to their own FWHM). G-Appendix.

Thus, If one uses an aplanatic NA=0.95 lens with either a two-belts DOE or five-belts DOE, can be generated linearly polarized subwavelength non-diffracting beams (optical needle with longitudinal polarization) along the z-axis (optical needle) or beams without divergence (constant waist) over its own FWHM (optical needle length). However, when one change the NA (Numerical Aperture) of the aplanatic lens, this generates a longitudinally polarized beams with different parameters, that is, waist and FWHM with different measurements, where both increase if the NA decreases, and in the same way, if the NA increases, both the waist and FWHM decrease.

Therefore, three longitudinally polarized beams generated by using an aplanatic lens of NA=0.90, NA=0.95 and NA=0.975 were simulated, which are shown in the following fig. (13).

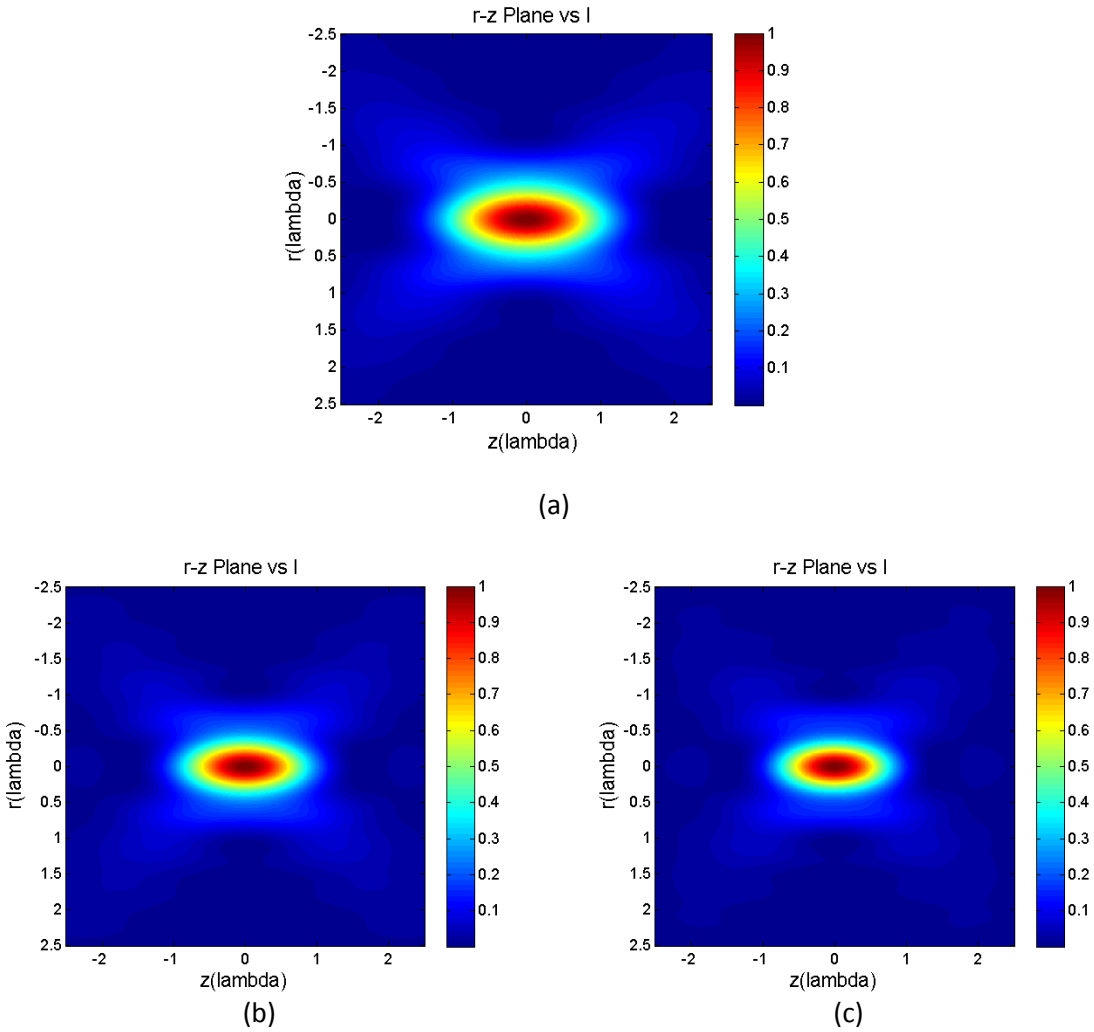

Figure 13. Longitudinally polarized beams generated by an aplanatic lens of (a) NA=0.90, (b) NA=0.95, and (c) NA=0.975, respectively. H-Appendix.

Similarly, if now one has an aplanatic lens of NA=0.90 and are further added individually the DOEs that are shown in the fig. (10), one can see that as in the fig. (12), the generated longitudinally polarized beam are shown in the figure 14, which increases its parameters (waist and FWHM) without changing its shape in comparison with the beams shown in the fig. (12), which are generated by the same DOE and an aplanatic lens of higher numerical aperture (NA=0.95).

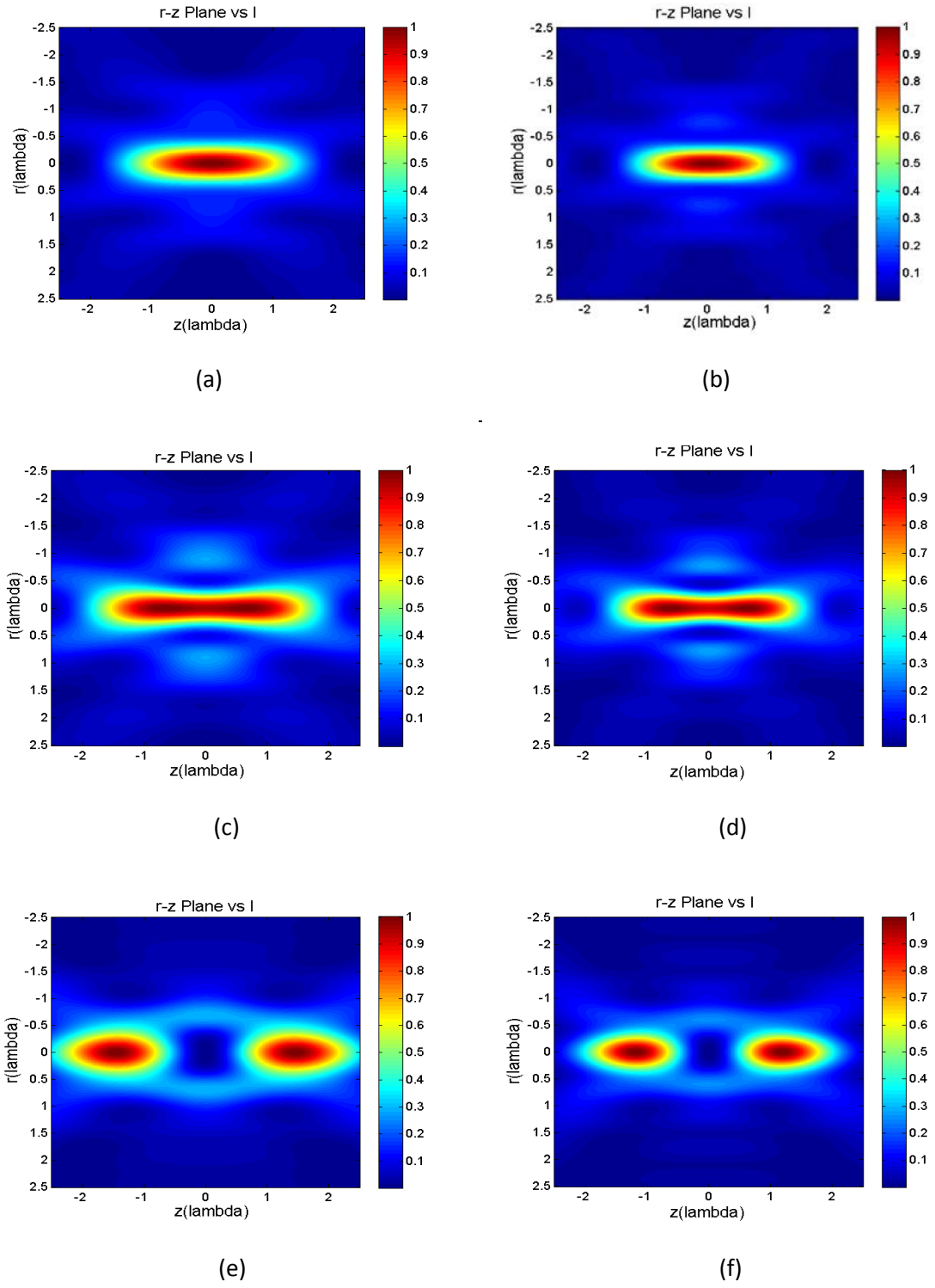

Figure 14. Longitudinally polarized beams generated by using an aplanatic lens and a DOE, both with different parameters, that is, widths ratio and numerical aperture of (a) r=26.392/64 and NA=0.90, (b) r=26.392/64 and NA=0.95, (c) r=32/64 and NA=0.90, (d) r=32/64 and NA=0.95, (e) r=46/64 and NA=0.90, (f) r=46/64 and NA=0.95, respectively. G-Appendix.

5.2. Experimental results

To the best of our knowledge, there exist a lack of reported results describing the experimental verification of several of the methods for generating specific focal fields, which are revised in this work. Therefore, an experimental method for verifying the existence of such beams is proposed here, which could prove the results obtained by numerical simulations, in this case the beams shown in the Fig. 14(c) and Fig. 14(e).

Let us consider beams are achieved by a beam with radial polarization, which are generated by using a polarization converter, and this is a commercial device named *S-WP* (S-Waveplate). Then, the radially polarized beam is transmitted through a specific parameters manufactured DOE (the designed and used DOEs are shown in the I-Appendix). The beam after the DOE is focused in an aplanatic MO (microscope objective) of NA=0.90 (see fig. (15)).

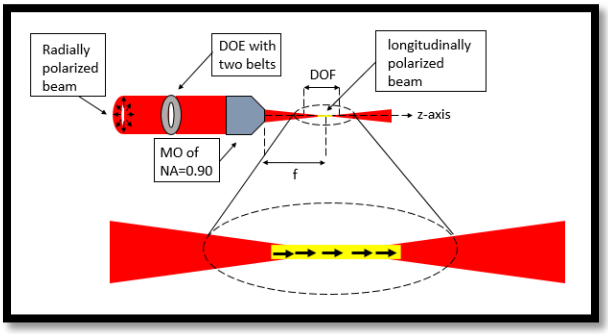

Figure 15. Optical arrangement proposed to be used in the laboratory.

Thus, when one has the radially polarized beam transmitted through a DOE, a longitudinally polarized beam is originated at the deep of focus region (DOF). Here we propose that the intensity distribution can be verified by using a vision system, which consists of a CMOS camera and an image forming lens, which are set over a translation stage to a fixed distance *di*, according to fig. (16).

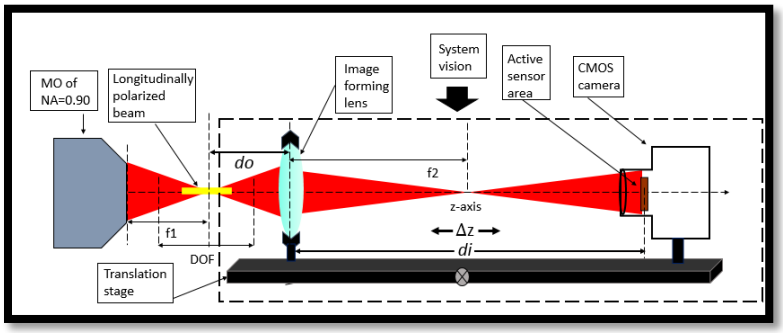

Figure 16. Vision system for the detection of a focal field

Thus, this system can be displaced along the z-axis in order to verify the focal field formed in the DOF. This field can be scanned registering the images of the object that is located at the distance d_o at different positions, given by equally spaced Δz steps of the translation stage, whose object position can be calculated by means of the Gauss' law, which can be represented as:

$$d_o = \frac{f_2 d_i}{d_i - f_2}. \tag{5.2.1}$$

Where d_o is the distance between the focal plane of the MO and the image forming lens, *di* is the fixed distance between the image forming lens and the CMOS camera sensor, and f_2 is the focal length of the image forming lens.

On the other hand, an important consideration in this proposed method is that the focal field should be registered, while the Δz steps of the translation stage are less than the FWHM of the longitudinal polarized beam formed in the DOF.

Chapter 6

Conclusions

---

6. Conclusions

The polarization is an important tool in optics and engineering, where many applications have reported focusing radially polarized vector-beams for generating longitudinally polarized beams, which can be obtained by using a lenses system of high NA (numerical aperture) or mirrors with very specific design. On the other hand, if one wants to get a non-diffracting longitudinal polarized beam with long FWHM (full width at half maximum) and subwavelength waist, that is, an ultra-long optical needle, one can use complementarily a diffractive optical element with concentric rings, where depending on the number of belts, the spacing between them and phase shift in each ring, will be the beam intensity profile, or in some cases, it is only change the size of the light source; similarly, if one wants to have additionally a beam with ultra-small (subwavelength) waist size, one can change the value of the NA of the used focusing lenses system, that is, if the value of the NA increases, the size of the beam waist decreases. However, not only decreases the size of the beam waist, but also its FWHM and consequently there will be a decrease of the zone to study and analyze with these beams, in this case, a decrease of the DOF (depth of field) of the used optical system.

Therefore, when a want to generate along the DOF an ultra-long optical needle with ultra-small waist, that is, a non-diffracting beam with high beam quality and subwavelength waist, one has to use a specific combination of different optical elements and an appropriate light source, where the parameters of these elements should be selected properly, since there is not a total dependence between these parameters and then is not possible to optimize at the same time all the beam parameters.

Appendix

A. Deduction of the field pattern radiated from a ULS

Given that a uniform linear source is a thin wire of L length that is aligned along the optical z axis, and whose electric current distribution within the wire is $I = I_0 e^{i(kR-\omega t)}$ Fig. (1). One can know the induction of magnetic field and by using the Ampere's law then know the electric field pattern radiated by the wire.

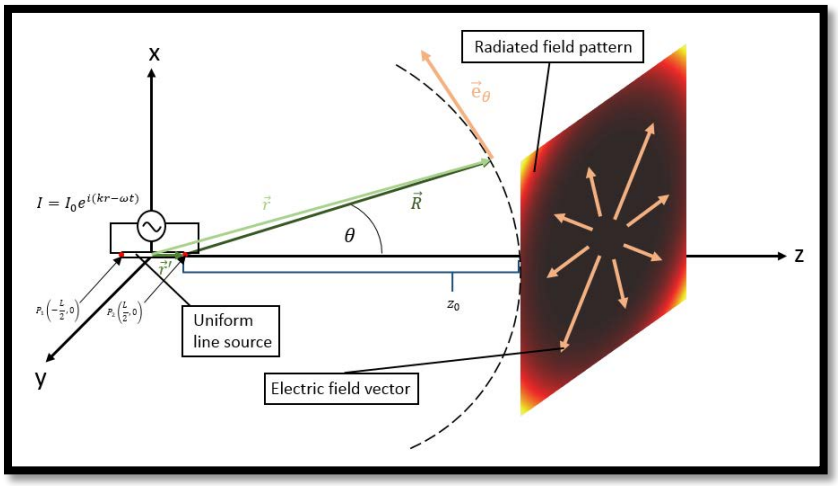

Figure 1. Radiation pattern by a thin wire of L length

Thus, in order to know $\vec{B}$, the Biot-Savart was used, which can be written as:

$$\vec{B}(\vec{r}) = \nabla \times \left[\frac{\mu_0}{4\pi}\oint_{-L/2}^{L/2} \frac{I(\vec{r}')d\vec{r}'}{R}\right]. \quad (1)$$

Where $\vec{r}'$ is the direction vector of the electric current, $\vec{r}$ is the vector from the wire to the observation point and R is $\|\vec{r} - \vec{r}'\|$.

If $\vec{r}' = z\hat{e}_z$ and $\vec{r} = x\hat{e}_x + y\hat{e}_y + z\hat{e}_z$, $R = \sqrt{r^2 + z^2 - 2zrcos(\theta)}$, and since the radiated field pattern is observed away from the wire, $r > z$ and then $R \approx r\sqrt{1 - 2cos(\theta)\left(\frac{z}{r}\right)}$.

Similarly, as z/r is a very small number, it is possible to approximate R to two terms of the Taylor series of $\sqrt{1-x}$ and consequently $R \approx r - zcos(\theta)$.

Therefore, the Eq. (1) can be rewritten as:

$$\vec{B}(\vec{r}) = \nabla \times \left[\frac{\mu_0}{4\pi}\oint_{-L/2}^{L/2} \frac{I_0 e^{i(kR-\omega t)}dz}{r}\,\hat{e}_z\right]. \quad (2)$$

Accordingly, first the $\vec{A}$ potential inside the square brackets of the Eq. (1) will calculated, so that $\vec{B}(\vec{r})$ can be expressed as:

$$\vec{B}(\vec{r}) = \nabla \times [A_z \hat{e}_z]. \tag{3}$$

With $A_z = \frac{\mu_0 I_0 L}{4\pi} \frac{e^{i(kr-\omega t)}}{r} \frac{sin\left[\frac{kL}{2}\cos(\theta)\right]}{\left[\frac{kL}{2}\cos(\theta)\right]}$.

In order to simplify and then solver the Eq. (3), $\vec{A}$ is written in spherical coordinates as shown below:

$$\vec{A} = A_z \cos(\theta)\, \hat{e}_r - A_z \sin(\theta)\, \hat{e}_\theta. \tag{4}$$

Thus, when $\nabla \times A$ is calculated, the $\vec{B}(\vec{r})$ can be rewritten as:

$$\vec{B}(\vec{r}) = \frac{1}{r}\left\{\frac{\partial}{\partial r}\left[r\left(-\frac{\mu_0 I_0 L e^{-i\omega t}}{4\pi}\frac{e^{ikr}}{r}\frac{sin\left[\frac{kL}{2}\cos(\theta)\right]}{\left[\frac{kL}{2}\cos(\theta)\right]}\right)\sin(\theta)\right]\right.$$
$$\left. - \frac{\partial}{\partial \theta}\left[\left(\frac{\mu_0 I_0 L e^{-i\omega t}}{4\pi}\frac{e^{ikr}}{r}\frac{sin\left[\frac{kL}{2}\cos(\theta)\right]}{\left[\frac{kL}{2}\cos(\theta)\right]}\right)\cos(\theta)\right]\right\}\hat{e}_\varphi. \tag{5}$$

In the same way, since $1/r^2$ is a very small number, the second term of the Eq. (5) can be neglected, so $\vec{B}(\vec{r})$ can be rewritten as:

$$\vec{B}(\vec{r}) = -i\frac{k}{r}\frac{\mu_0 I_0 L}{4\pi} e^{i(kr-\omega t)} \sin(\theta) \frac{sin\left[\frac{kL}{2}\cos(\theta)\right]}{\left[\frac{kL}{2}\cos(\theta)\right]}\hat{e}_\varphi. \tag{6}$$

Therefore, in order to know $\vec{E}(\vec{r})$, the Ampere's law $\left(\nabla \times \vec{B} = \mu_0 \varepsilon_0 \frac{\partial \vec{E}}{\partial t}\right)$ is used, where first $\nabla \times \vec{B}(\vec{r})$, which can be written as:

$$\nabla \times \vec{B}(\vec{r}) = -\frac{\mu_0 I_0 L k^2}{4\pi r} e^{i(kr-\omega t)} \sin(\theta) \frac{sin\left[\frac{kL}{2}\cos(\theta)\right]}{\left[\frac{kL}{2}\cos(\theta)\right]}\hat{e}_\theta. \tag{7}$$

Finally, If $\nabla \times \vec{B}(\vec{r})$ is known, $\vec{E}(\vec{r}) = c^2 \int \nabla \times \vec{B}(\vec{r})\, dt\, \hat{e}_\theta$, which can be written as:

$$\vec{E}(\vec{r}) = -i\frac{\mu_0 I_0 L \omega}{4\pi r} e^{i(kr-\omega t)}\, sin(\theta) \frac{sin\left[\left(\frac{kL}{2}\right)cos(\theta)\right]}{\left(\frac{kL}{2}\right)cos(\theta)}\hat{e}_\theta. \tag{8}$$

B. FWHM of a flat-top beam

```
%%% Length of the optical needle
clc
close all
%% parameters
l=1;%lambda
A=1;
k=2*pi/l;
n=10;%length of the uniform linear source
L=n*l;
c=1;
```

```
r=0; % r coordinate
angle=90;
t=linspace(0,angle*pi/180,1000);

IEZI=0;

for z=-6:0.01:6;

    a=( (c.*sin(t).*sin((k*L/2).*cos(t))./((k*L/2).*cos(t)))
.* ((cos(0)).^(1/2))...
    .* (sin(t).^2) .* (besselj(0,k* (r) .*sin(t))) .*
(exp(1i*k*z.*cos(t))) ) ;
    ez=trapz(t,a);
    EZ=2*A*1i*ez;

    IEZI=[IEZI, (imag(EZ))^2];

end
z=-6:0.01:6;
    figure(1);
    %% beam profile
    plot(z,IEZI(2:end),'r.');
    %%  normalized beam profile
    IEZIM=max(max(IEZI));
    IN=IEZI/IEZIM;
    figure(2);
    plot(z,IN(2:end),'g.');

    title('Normalized I vs z')
    xlabel('z(lambda)')
    ylabel('Intensity on the optical axis')
    hold on;
    drawnow
```

C. Waist of a non-diffracting beam

```
%%% Optical needle with an ULS
%%
clear,clc,close all,
%% Main parameters

l=1;      % wavelength
A=1;      % constant amplitude
k=2*pi/l; % wavenuber
n=10;     % length parameter of the uniform line source
L=n*l;    % length of uniform line source
```

```
c=1;      % constant related to the uniform line source
strength
%% integration variable t for the integral (trapz)
t=linspace(0,90*pi/180,1000);
I=zeros(1,1201);
for r=-1:0.01:1
    Iz=0;
    Ir=0;
    for z=-6:0.01:6;

        F=c.*sin(t).*sin((k*L/2).*cos(t))./((k*L/2).*cos(t));

        ar=(     (     F     ) ...
        .* (sin(2*t)/2) .* (besselj(1,k* (r) .*sin(t))) .*
(exp(1i*k*z.*cos(t))) ) ;
        er=trapz(t,ar);
        ER=2*A*er;
        Ir=[Ir real(abs(ER).^2)];
        az=(     (     F     ) ...
        .* (sin(t).^2) .* (besselj(0,k* (r) .*sin(t))) .*
(exp(1i*k*z.*cos(t))) ) ;
        ez=trapz(t,az);
        EZ=2*A*1i*ez;
        Iz=[Iz imag(EZ)^2];
    end
    Iz=Iz(2:end);
    Ir=Ir(2:end);
    I=[I;Iz+Ir];
    z=-6:0.01:6;

end
I=I(2:end,:);
r=-1:0.1:1; % invert axis
figure(1)
imagesc(z,r,I),colormap hot;
 title('r-z Plane vs I ')
    xlabel('z(lambda)')
    ylabel('r(lambda)')
```

D. Length of the optical needle for the BG beam and by using a DOE with five-belts

```
%% Length of the optical needle for the BG beam
clc
close all
%% parameters
l=1;%lambda
```

```
A=1;
k=2*pi/l;

r=0; % r coordinate
angle=asin(0.95); % acceptance angle and numerical aperture
t=linspace(0,angle,1000);

IEZI=0;
%%
for z=-2.50:0.01:2.50;

    beta=1;
    gamma=1;
        BG=exp(  -(beta^2) * (sin(t)/sin(asin(angle))).^2   )
.* ...
            besselj(1,2*gamma*(sin(t)/sin(asin(angle))));


%% with five optimized belts

%         interval1=t>=0 & t<4.96*pi/180; %r1
%         interval2=t>=21.79*pi/180 & t<34.25*pi/180; %r3
%         interval3=t>=46.87*pi/180 & t<=asin(angle); %r5
%         maskPositive=interval1 + interval2 + interval3;
%         maskNegative=~maskPositive;
%         T=maskPositive-maskNegative;

%% with five equally spaced belts

%         interval1=t>=0 & t<angle/5; %r1
%         interval2=t>=angle*2/5 & t<angle*3/5; %r3
%         interval3=t>=angle*4/5 & t<=angle; %r5
%         maskPositive=interval1 + interval2 + interval3;
%         maskNegative=~maskPositive;
%         T=maskPositive-maskNegative;

%% without DOE

%     T=1 ;


%% evaluation of the integral
    a=( ( T.* BG ) .* ((cos(t)).^(1/2))...
    .* (sin(t).^2) .* (besselj(0,k* (r) .*sin(t))) .*
(exp(1i*k*z.*cos(t))) ) ;

    ez=trapz(t,a);
```

```
    EZ=2*A*1i*ez;

    IEZI=[IEZI, real(abs(EZ).^2)];

end
%%
z=-2.50:0.01:2.50;
    figure(1);
    %% beam profile
    plot(z,IEZI(2:end),'r.');

 %%  normalized beam profile
    IEZIM=max(max(IEZI));
    IN=IEZI/IEZIM;
    figure(2);
    plot(z,IN(2:end),'g.');

    title('Normalized I vs z')
    xlabel('z(lambda)')
    ylabel('Intensity on the optical axis')
    hold on;
    drawnow
```

E. Length of the optical needle for the BG beam and by using a DOE with two-belts

```
%% Length of the optical needle for the BG beam
clc
close all
%% parameters
l=1;%lambda
A=1;
k=2*pi/l;

r=0; % r coordinate
angle=asin(0.95); % acceptance angle and numerical aperture
t=linspace(0,angle,1000);

IEZI=0;
%%
for z=-2.50:0.01:2.50;

    beta=1;
    gamma=1;
        BG=exp(  -(beta^2) * (sin(t)/sin(asin(angle))).^2   )
.* ...
```

```
            besselj(1,2*gamma*(sin(t)/sin(asin(angle))));


%% with five optimized belts

%         interval1=t>=0 & t<4.96*pi/180; %r1
%         interval2=t>=21.79*pi/180 & t<34.25*pi/180; %r3
%         interval3=t>=46.87*pi/180 & t<=asin(angle); %r5
%         maskPositive=interval1 + interval2 + interval3;
%         maskNegative=~maskPositive;
%         T=maskPositive-maskNegative;

%% with five equally spaced belts

%         interval1=t>=0 & t<angle/5; %r1
%         interval2=t>=angle*2/5 & t<angle*3/5; %r3
%         interval3=t>=angle*4/5 & t<=angle; %r5
%         maskPositive=interval1 + interval2 + interval3;
%         maskNegative=~maskPositive;
%         T=maskPositive-maskNegative;

%% without DOE

%     T=1 ;


%% evaluation of the integral
    a=( ( T.* BG ) .* ((cos(t)).^(1/2))...
    .* (sin(t).^2) .* (besselj(0,k* (r) .*sin(t))) .*
(exp(1i*k*z.*cos(t))) ) ;

    ez=trapz(t,a);
    EZ=2*A*1i*ez;

    IEZI=[IEZI, real(abs(EZ).^2)];

end
%%
z=-2.50:0.01:2.50;
    figure(1);
    %% beam profile
    plot(z,IEZI(2:end),'r.');

 %%  normalized beam profile
    IEZIM=max(max(IEZI));
    IN=IEZI/IEZIM;
    figure(2);
```

```
    plot(z,IN(2:end),'g.');

    title('Normalized I vs z')
    xlabel('z(lambda)')
    ylabel('Intensity on the optical axis')
    hold on;
    drawnow
```

F. Optical needle by using a five-belts DOE

```
%% OPTICAL NEEDLE WITH A B-G BEAM

tic %(initial time)
close all
l=1;      % wavelength
A=1;      % amplitude  constant
k=2*pi/l; % wavenuber
% n=10;     % length parameter of uniform line source
% L=n*l;    % length of uniform line source
c=1;      % constant related to the uniform line source
strength

alfa=0.95; % NA
t=linspace(0,asin(alfa),1000);
i_s=6; % image size
I=zeros(1, 200*i_s + 1 );

for r=-2.5:0.01:2.5;
    Iz=0;
    Ir=0;
    for z=-1*i_s:0.01:i_s;

%% light source
        beta=1;
        gamma=1;
        BG=exp(  -(beta^2) * (sin(t)/sin(asin(alfa))).^2   )
.* ...
            besselj(1,2*gamma*(sin(t)/sin(asin(alfa))));
% % % parameters of the DOE


% % five belts with optimazed parameters
%         interval1=t>=0 & t<4.96*pi/180; %r1
%         interval2=t>=21.79*pi/180 & t<34.25*pi/180; %r3
%         interval3=t>=46.87*pi/180 & t<=asin(alfa); %r5
%         maskPositive=interval1 + interval2 + interval3;
```

```
%         maskNegative=~maskPositive;
%         T=maskPositive-maskNegative;

% % five equally spaced belts
%         interval1=t>=0 & t<asin(alfa)/5; %r1
%         interval2=t>=asin(alfa)*2/5 & t<asin(alfa)*3/5; %r3
%         interval3=t>=asin(alfa)*4/5 & t<=asin(alfa); %r5
%         maskPositive=interval1 + interval2 + interval3;
%         maskNegative=~maskPositive;
%         T=maskPositive-maskNegative;


% % % without  DOE

  T=1;
%% Richard-Wolf vectorial diffraction integral
        ar=(     T.* (     BG     ) ...
        .* (sin(2*t)/2) .* (besselj(1,k* (r) .*sin(t))) .*
(exp(1i*k*z.*cos(t))) ) ;
        er=trapz(t,ar);
        ER=2*A*er;
        Ir=[Ir real(abs(ER).^2)];
        az=(     T.* (     BG     ) ...
        .* (sin(t).^2) .* (besselj(0,k* (r) .*sin(t))) .*
(exp(1i*k*z.*cos(t))) ) ;
        ez=trapz(t,az);
        EZ=2*A*1i*ez;
        Iz=[Iz real(abs(EZ).^2)]; %  imag(EZ)^2
    end
    Iz=Iz(2:end);
    Ir=Ir(2:end);
    I=[I;Iz+Ir];
    z=-1*i_s:0.01:i_s;

end
I=I(2:end,:)/max(max(  I(2:end,:)  ));
r=-2.5:0.1:2.5;
figure(2)
imagesc(z,r,I),colormap jet;colorbar;
 title('r-z Plane vs I ')
    xlabel('z(lambda)')
    ylabel('r(lambda)')
    axis 'square'

 toc  % (final time)
```

G. Optical needle by using a two-belts DOE

```
%% OPTICAL NEEDLE WITH A B-G BEAM

tic %(initial time)
close all
l=1;      % longitud de onda
A=1;      % amplitude  constant
k=2*pi/l; % wavenuber
% n=10;     % length parameter of uniform line source
% L=n*l;    % length of uniform line source
c=1;      % constant related to the uniform line source
strength

alfa=0.95; % NA
t=linspace(0,asin(alfa),1000);
i_s=2.5; % image size
I=zeros(1, 200*i_s + 1 );

for r=-2.5:0.01:2.5;
    Iz=0;
    Ir=0;
    for z=-1*i_s:0.01:i_s;

%% light source
        beta=1;
        gamma=1;
        BG=exp(  -(beta^2) * (sin(t)/sin(asin(alfa))).^2   )
.* ...
            besselj(1,2*gamma*(sin(t)/sin(asin(alfa))));

% % % parameters of the DOE



% % two equally spaced belts with ratio 1/2 a 1/2
%         interval1=t>=0 & t<asin(alfa)/2; %r1
% %         interval2=t>=asin(alfa)*2/5 & t<asin(alfa)*3/5;
%r3
% %         interval3=t>=asin(alfa)*4/5 & t<=asin(alfa); %r5
%         maskPositive=interval1
%         maskNegative=~maskPositive;
%         T=maskPositive-maskNegative;


% % two belts with variable r (radius)
% radius=26.392;
```

```
% % 2 BELTS WITH RATIO OF RADIUS/64 TO (RADIUS-64)/64.
%         interval1=t>=0 & t<asin(alfa)*radius/64; %r1
% %         interval2=t>=asin(alfa)*2/5 & t<asin(alfa)*3/5;
%r3
% %         interval3=t>=asin(alfa)*4/5 & t<=asin(alfa); %r5
%         maskPositive=interval1
%         maskNegative=~maskPositive;
%         T=maskPositive-maskNegative;



% % % without  DOE

  T=1;
%% Richard-Wolf vectorial diffraction integral
        ar=(     T.* (     BG     ) ...
        .* (sin(2*t)/2) .* (besselj(1,k* (r) .*sin(t))) .*
(exp(1i*k*z.*cos(t))) ) ;
        er=trapz(t,ar);
        ER=2*A*er;
        Ir=[Ir real(abs(ER).^2)];
        az=(     T.* (     BG     ) ...
        .* (sin(t).^2) .* (besselj(0,k* (r) .*sin(t))) .*
(exp(1i*k*z.*cos(t))) ) ;
        ez=trapz(t,az);
        EZ=2*A*1i*ez;
        Iz=[Iz real(abs(EZ).^2)]; %  imag(EZ)^2
    end
    Iz=Iz(2:end);
    Ir=Ir(2:end);
    I=[I;Iz+Ir];
    z=-1*i_s:0.01:i_s;

end
I=I(2:end,:)/max(max(  I(2:end,:)  ));
r=-2.5:0.1:2.5;
figure(2)
imagesc(z,r,I),colormap jet;colorbar;
 title('r-z Plane vs I ')
    xlabel('z(lambda)')
    ylabel('r(lambda)')
    axis 'square'

 toc  % (final time)
```

H. Longitudinally polarized beam with variable NA

```
%% OPTICAL NEEDLE WITH A B-G BEAM

tic %(initial time)
close all
l=1;      % longitud de onda
A=1;      % amplitude  constant
k=2*pi/l; % wavenuber
% n=10;     % length parameter of uniform line source
% L=n*l;    % length of uniform line source
c=1;      % constant related to the uniform line source
strength

alfa=0.95; % NA
t=linspace(0,asin(alfa),1000);
i_s=2.5; % image size
I=zeros(1, 200*i_s + 1 );

for r=-2.5:0.01:2.5;
    Iz=0;
    Ir=0;
    for z=-1*i_s:0.01:i_s;

%% light source
        beta=1;
        gamma=1;
        BG=exp(  -(beta^2) * (sin(t)/sin(asin(alfa))).^2   )
.* ...
            besselj(1,2*gamma*(sin(t)/sin(asin(alfa))));

%% Richard-Wolf vectorial diffraction integral
        ar=(     1.* (     BG     ) ...
        .* (sin(2*t)/2) .* (besselj(1,k* (r) .*sin(t))) .*
(exp(1i*k*z.*cos(t))) ) ;
        er=trapz(t,ar);
        ER=2*A*er;
        Ir=[Ir real(abs(ER).^2)];
        az=(     T.* (     BG     ) ...
        .* (sin(t).^2) .* (besselj(0,k* (r) .*sin(t))) .*
(exp(1i*k*z.*cos(t))) ) ;
        ez=trapz(t,az);
        EZ=2*A*1i*ez;
        Iz=[Iz real(abs(EZ).^2)]; %  imag(EZ)^2
    end
    Iz=Iz(2:end);
    Ir=Ir(2:end);
    I=[I;Iz+Ir];
    z=-1*i_s:0.01:i_s;
```

```
end
I=I(2:end,:)/max(max(  I(2:end,:)  ));
r=-2.5:0.1:2.5;
figure(2)
imagesc(z,r,I),colormap jet;colorbar;
 title('r-z Plane vs I ')
    xlabel('z(lambda)')
    ylabel('r(lambda)')
    axis 'square'

 toc  % (final time)
```

I. Two-belts DOEs Designs

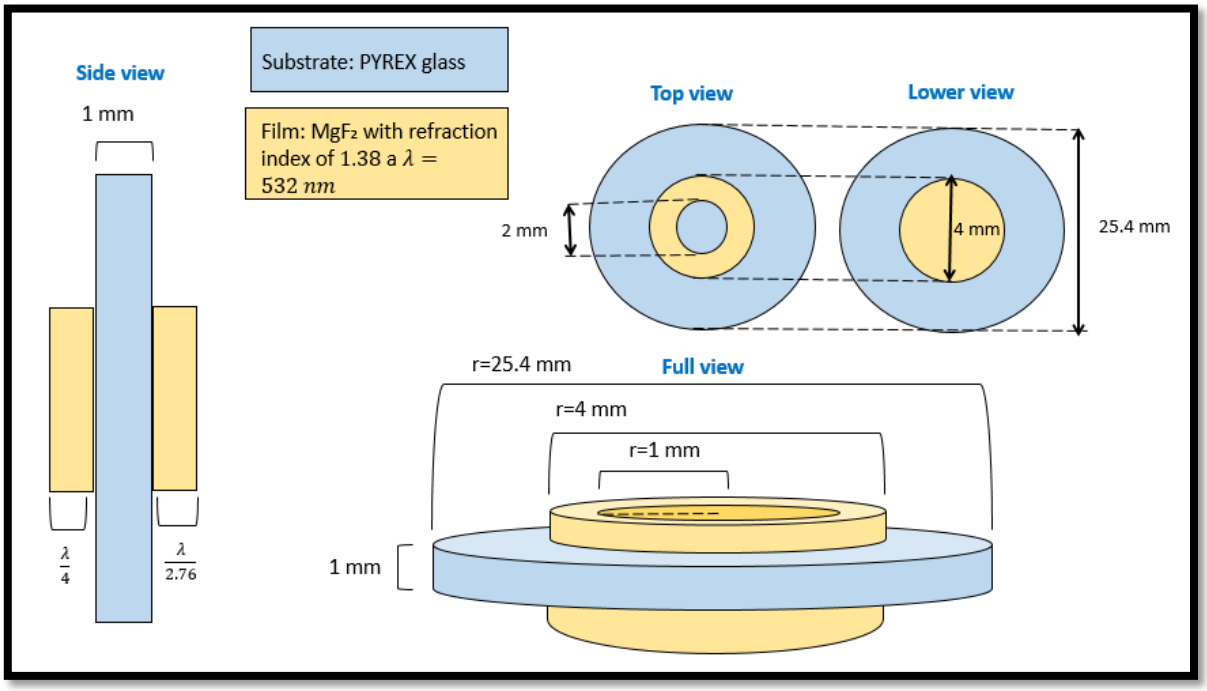

Figure 1. Two-belts DOE with ratio r of 32/64

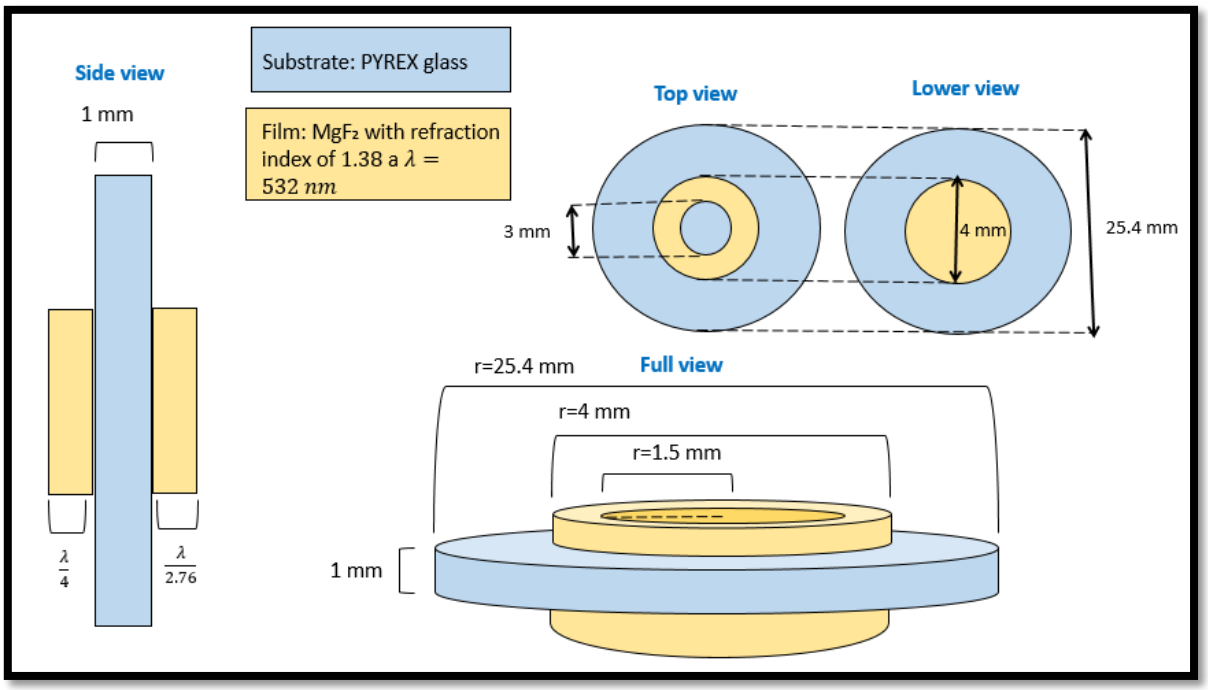

Figure 2. Two-belts DOE with ratio r of 46/64

Bibliography

1. H. F. Wang, L. P. Shi, B. Lukyanchuk, C. Sheppard, and C. T. Chong, "Creation of a needle of longitudinally polarized light in vacuum using binary optics," Nat. Photonics **2**(8), 501–505 (2008).
2. Y. Yu and Q. Zhan, "Optimization-free optical focal field engineering through reversing the radiation pattern from a uniform line source," Opt. Express. **23**(6), 7527-7534 (2015)
3. E. Wolf, "Electromagnetic diffraction in optical systems I. An integral representation of the image field," Proc. R. Soc. Ser. A **253**, 349–357 (1959).
4. B. Richards and E. Wolf, "Electromagnetic diffraction in optical system II. Structure of the image field in an aplanatic system," Proc. R. Soc. Ser. A **253**, 358–379 (1959).
5. K. Huang, P. Shi, X. L. Kang, X. B. Zhang, and Y. P. Li, "Design of DOE for generating a needle of a strong longitudinally polarized field," Opt. Lett. **35**(7), 965–967 (2010).
6. N. Bokor and N. Davidson, "Toward a spherical spot distribution with 4pi focusing of radially polarized light," Opt. Lett. **29**(17), 1968–1970 (2004).
7. S. Yan, B. Yao, and R. Rupp, "Shifting the spherical focus of a 4Pi focusing system," Opt. Express **19**(2), 673–678 (2011).
8. D. G. Hall, "Vector-beam solutions of Maxwell's wave equation", Opt. Lett. **21**, 9-11 (1996).
9. K. S. Youngworth and T. G. Brown, "Focusing of high numerical aperture cylindrical-vector beams," Opt. Express **7**(2), 77–87 (2000).
10. W. L. Stutzman and G. A. Thiele, Antenna Theory and Design, 2nd Edition (J. Wiley, 1998).
11. J. Liu, M. Ai, J. Tan, R. Wang, and X. Tan, "Focusing of cylindrical-vector beams in elliptical mirror based system with high numerical aperture," Opt. Commun, **305**, 71–75 (2013).
12. M. Lieb and A.Meixner, "A high numerical aperture parabolic mirror as imaging device for confocal microscopy," Opt. Express **8**(7), 458–474 (2001).
13. H. Dehez, A. April, and M. Piche, "Needles of longitudinally polarized light: guidelines for minimum spot size and tunable axial extent," Opt. Express **20**(14), 14891–14905 (2012).
14. T. Liu, J. Tan, J. Lin, and J. Liu, "Generating super-Gaussian light needle of 0.36λ beam size and pure longitudinal polarization," Opt. Eng. **52**(7), 074104 (2013).
15. J. Lin et al., "Achievement of longitudinally polarized focusing with long focal depth by amplitude modulation," Opt. Lett. **36**(7), 1185–1187 (2011).
16. W. Chen and Q. Zhan, "Creating a spherical focal spot with spatially modulated radial polarization in 4Pi microscopy," Opt. Lett. **34**(16), 2444–2446 (2009).
17. J. Wang, W. Chen, and Q. Zhan, "Three-dimensional focus engineering using dipole array radiation pattern", Opt. Commun. **284**(12), 2668–2671 (2011).
18. A. Ashikin and J. Z. Dziedzic, "Optical trapping and manipulation of viruses and bacteria" Science. **235**, 1517-1520 (1987).

19. Q. Zhan, "Cylindrical vector beams: from mathematical concepts to applications," Adv. Opt. Photon **1**(1), 1–57 (2009).
20. S. Bravo Yuste, Métodos matemáticos avanzados para científicos e ingenieros, Edición electrónica: Pedro Cid, S.A. (Universidad de Extremadura. Servicio de Publicaciones, 2006).